Eindhoven University of Technology

MASTER

Development of Fischer Tropsch foam catalyst and reactor development diffusion limitations for FTS foam catalyst

van der Linden, C.

Award date:
2017

Link to publication

Disclaimer
This document contains a student thesis (bachelor's or master's), as authored by a student at Eindhoven University of Technology. Student theses are made available in the TU/e repository upon obtaining the required degree. The grade received is not published on the document as presented in the repository. The required complexity or quality of research of student theses may vary by program, and the required minimum study period may vary in duration.

General rights
Copyright and moral rights for the publications made accessible in the public portal are retained by the authors and/or other copyright owners and it is a condition of accessing publications that users recognise and abide by the legal requirements associated with these rights.

- Users may download and print one copy of any publication from the public portal for the purpose of private study or research.
- You may not further distribute the material or use it for any profit-making activity or commercial gain

Department of Chemical Engineering and Chemistry
Chemical Reactor Engineering
De Rondom 70, 5612 AP Eindhoven
P.O. Box 513, 5600 MB Eindhoven
The Netherlands
www.tue.nl

Author
C. van der Linden

Date
August 10, 2017

Version
1.0

Development of Fischer Tropsch foam catalyst and reactor development

Diffusion limitations for FTS foam catalyst

Master Thesis

Submitted in partial fulfillment of the requirements for
the degree of Master of Science
in the Department of Chemistry and Chemical Engineering
at Eindhoven University of Technology

Abstract

The Fischer Tropsch synthesis is used to convert syngas to hydrocarbons. The main issue for the reaction are the diffusional restrictions in the porous network of FT catalysts which can strongly affect the product selectivity.

In this work, Co-based catalysts on $\gamma-$alumina were synthesized and tested on FTS activity with the aim to evaluate the effect of the intra-particle mass transfer limitation on the process selectivity for foam catalysts as well as conventional powder supported catalysts. Several foam catalysts were made by washcoating the solid foams, which resulted in washcoat thicknesses of 7, 17 and 30 μm. The prepared foam catalysts were compared to powder catalysts with particle sizes of 50, 75 and 100 μm.

Activity tests on the powder catalyst showed activity FTS products while showing water gas shift activity in the form of CO_2 formation. Activity tests of the foam catalysts showed no measurable product formation and activity in water gas shift. TGA measurements on both foam and powder catalysts showed carbon formation on the catalyst support. While the produced catalysts were active for FTS, the catalysts were not optimally produced leading to no observed effect for intra particle diffusion limitations.

Additionally to the activity testing a numerical model was made to give more insight in intra-particle diffusion limitations the model shows the effect of intra-particle diffusion limitations on the different catalyst support. Diffusion limitations occured for the foam catalyst while for the powder catalysts no intra-particle diffusion limitations were observed.

Contents

Chapter 1

Introduction

Fischer Tropsch synthesis (FTS) is a process to produce hydrocarbons out of syngas from various different sources like shale gas, coal and other natural resources. In recent years the industrial interest in FTS has increased due to low oil prices. At low oil prices FTS is not economically competitive with more traditional processes such as oil cracking. However when oil prices are high the industry seeks for alternatives. In 2006 the American oil industry was interested in shale gas as alternative to oil, due to high oil prices. Investments in shale gas where at a all time high causing interest in FTS to rise. The FTS can be used to convert syngas in higher value products. Since 2006 the oil price has dropped and interest in FTS has dropped as well. From an environmental aspect FTS can be used to convert syngas from biomass to hydrocarbons, creating environmentally friendly fuels which in the current energy crisis is of high value.

$$n\mathrm{CO} + 2n\mathrm{H_2} \rightarrow (-\mathrm{CH_2}-)_n + n\mathrm{H_2O} \tag{R1}$$

Traditionally FTS is carried out in a slurry bubble column (SBC) or a packed bed reactor (PBR). Both reactor types contain powder supported catalysts where the reaction takes place in the internal volume of the catalyst. The general chemical reaction is shown in equation R1. The catalysts used contain either cobalt or iron as active metal and are used on various types of supports like γ-alumina, silica and carbon [1]. The Fischer Tropsch reaction is a polymerization reaction where hydrocarbon chains $-(CH_2)_n-$ are produced. FTS follows the chain growth probability mechanism of Anderson Schultz Flory (ASF) [2]. Depending on the concentration ratio of the reactants, temperature and pressure the chain growth probability of the FTS is influenced. The concentration ratio of the reactants hydrogen (H_2) and carbon monoxide (CO) is also referred as the hydrogen to carbon ratio H_2/CO. Selectivity to middle distillates of chain length $C5$ to $C9$ are of high value and therefore wanted products in FTS is for products with a chain longer than five, $C5+$ products. Longer products could be refined to the wanted length.

One of the biggest concerns in the design of a FTS type reactor are intra-particle diffusion limitations. These diffusion limitations occur because the diffusion of reactants H_2 and CO through the particle differs from one another. The diffusion of H_2 is much faster than CO leading to a local difference in H_2/CO ratio, which has a large effect on the product selectivity of the reaction

[2, 3, 4]. The larger the size of the catalyst, the larger the effects of diffusion limitations [2, 4]. When the H_2/CO ratio is larger than four, the FTS produces mainly methane. Methane is in the case of shale gas the source for syngas and is therefore an unwanted product. When long hydrocarbons are formed, the catalyst pores are slowly filled with wax products decreasing the diffusion rate of reactants in the particle which is the cause of intra-particle diffusion limitations.

Another factor in FTS intra-particle diffusion limitations is the effect of temperature. The FTS reaction is an exothermic reaction which leads to a local temperature rise causing hotspot formation. At higher temperatures the reaction rate increases which leads to a depletion of CO and in a smaller extend H_2 in the particle causing an increase in the $H2/CO$ ratio even more [5].

Over the years there has been extensive research in FTS intra-particle diffusion limitation. In a paper of Yang et al [6] mass transfer limitations on fixed-bed for FTS was investigated by changing synthesis gas superficial velocity, catalyst pellet size, and catalyst amount. They found that compared to small catalyst particles, larger particles have a larger selectivity for $C5+$ products due to re-adsorption of olefins. The production of wax hydrocarbons was lower due to diffusion limitations in larger particles. They suggested using large pelletized particles to limit pressure drop over the reactor. Shell has conducted a study where they varied the catalyst particle size from 0.2 to 2.6 mm to find out the effect of intra-particle diffusion limitations on the conversion of syngas without considering selectivities. Variation of catalyst particle size in the range showed that the conversion of synthesis gas decreases considerably when the average particle size is increased [7].

The effect of catalyst support material plays an important role in the activity and selectivity of the FTS. Rytter et al [8] conducted a literature study on the effect of the catalyst support on FTS selectivity and productivity with an emphasis on cobalt on alumina type supports. They found that the alumina has a large interaction with active phase leading to a harder reducibility of the active phase. For small support sizes the pore size of the support is smaller. Smaller pores lead to smaller cobalt crystals which leads to a shift in productivity and selectivity for FTS due to harder reducibility of the active phase. For alumina catalyst diameters up to 100 μm, diffusion limitations in terms of selectivity and productivity are absent. The same results were also found in a review paper of Khodakov [9]. For iron type catalysts similar effects were observed [10].

It is also possible to influence diffusion limitations by altering the pore structure of the catalyst itself. A study of Becker et al [11] used bimodal pores to relief the catalyst of transport limitations due to wax formation. First micro-pores were impregnated with a cobalt/ruthenium active phase after which larger meso-pores were made in the catalyst to decrease diffusion length in wax filled micro-pores. By comparing bimodal catalysts with normal catalysts they showed that using bi modal catalyst decrease the conversion of CO by 50-70% but increases the selectivity of $C5+$ products and decreases methane formation. The lower conversion is due to less catalyst per volume and the higher selectivity for $C5+$ is due to the decrease in diffusion length in the micro pores. These results were also obtained by modeling catalyst particles with transport pores [12].

Fratalocchia et al [13] compared pelleted eggshell catalysts with a diameter of 600 μm to powder catalysts with a particle size distribution of 100-75 μm. They found that the pellets have a higher CO conversion and selectivity to $C5+$ products. This is due to longer diffusion paths so that re-adsorption of olefins can occur, increasing chain lengths of products. Another study of Ishihara et al. created bi modal pores by filling mesopores with a ZrO_2 sols creating micropores. These micropores were used to enlarge the dispersion of Cobalt active phase. The cobalt active phase is deposited on the support surface in the micropores. Compared to normal powder catalysts the bi modal catalyst showed 83 % increase in CO conversion and 9.8% decrease of methane selectivity. The increase of CO conversion was due to the fine dispersion of cobalt nanoparticles. The enhanced selectivity was due to the deep small pore facilitated the mesopores. This promoted olefin re-adsorption which decreased the selectivity for methane and enlarged chain growth.

Alternatively FTS can also be carried out in micro reactors. Ying et al. [14] performed FTS in microreactors where the walls were coated with a γ-alumina on which a cobalt catalyst was deposited. Results show higher conversion of CO and lower methane selectivity. This was due to enhancement in mass and heat transfer. A simple way to control intra-particle diffusion limitations is to use smaller catalyst particles. However, using smaller particles leads to a larger pressuredrop in PBR reactors and for SBC reactors using smaller particles leads to a more difficult separation of catalyst from slurry phase. Basseem et al modeled the FTS catalysts and found an optimal particle size of 1.1 mm for controlling pressure drop in FTS PBR's [15]. Using particles in the mm scale results in a large reduction of productivity. Another alternative is changing the catalyst type from powder catalysts to foam catalysts.

By applying structured foam catalysts small diffusion paths can be obtained without pressure drop or catalyst removal implications. Another advantage of applying metallic foam catalyst is the eggshell shape of the catalyst. The inner part of the foam structure is metallic which contributes in a better removal of heat in the catalyst. The thin layer of catalyst on the foam is advantageous for mass transfer of the catalyst as well. These advantages come at the cost of having less catalyst per reactor volume resulting in a lower productivity for a similar sized reactor. However using eggshell catalysts and mesoporous powder catalyst suffers from the same loss in productivity as well. In a study of Yang et al cobalt on alumina foam catalysts was compared to uniform cobalt pellets. Results showed that the foam catalyst exhibit a higher $C5+$ productivity and lower methane formation due to the absence of intra-particle diffusion limitations and absence of hotspot formation in the catalytic foam [4]. Most studies showcase the effect of diffusion limitations on powder catalysts by comparing one small particle size with a fairly large one. Modeling of small particle catalysts showed that diffusion limitations occur for particle diameters larger than 10 μm [16]. Which implies that diffusion limitations on foam catalysts could occur as well.

The goal of this study is to find out the effect of intra-particle diffusion limitations on the selectivity and productivity of foam catalysts in the FTS. Another goal is to find out how what the effect of intra-particle diffusion limitations of foam catalysts are compared to powder catalysts. To achieve these goals several foam and powder catalysts were made and tested in a PBR. In

parallel a mathematical model of the system is made for comparison and to provide theoretical insight into the mechanisms that influence the FTS conversions and selectivity.

Chapter 2

Experimental

In this study several powder and foam supported catalysts were prepared to give insight in the performance of foam catalysts in comparison to more conventional catalyst types. As catalyst cobalt supported on γ-alumina was used. Five different powder type catalysts with different particle sizes were produced. The foams used in the reactor were 2 cm long cylinders with a diameter of 1 cm. Figure 2.1 shows the metallic foam on which the catalyst was applied:

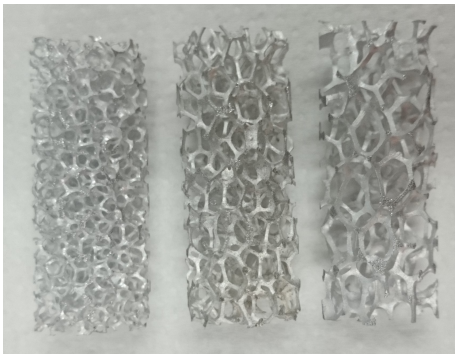

Figure 2.1: Foam pieces used in the FTS: 10,20 and 40 ppi

For the foam catalysts a pore density of 20 pores per inch (ppi) was used. In total 9 foams were produced with 3 different washcoat thicknesses. The catalysts were characterized thoroughly and used for activity testing in the setup. This chapter describes the preparation methods, characterization techniques, the setup and activity test which were employed in the study.

2.1 Preparation of powder catalyst

The powder catalysts were prepared in the following steps:

1. Sizing of catalyst support:
   Different particle sizes for the catalyst support were needed to give insight in diffusion limitation for powder catalysts. Different fractions of particle sizes were made from com-

mercial γ-alumina with a particle size of 200 μm. The particle size was modified by pelletizing the alumina subsequently the alumina was crushed and sieved using sieves of 150, 125, 100, 75 and 50 μm. This method resulted in the following fractions of the catalyst support: (150-125 μm),(125-100 μm),(100-75 μm),(75-50 μm) and(50-0 μm).

2. Impregnation of the active phase:
   Deposition precipitation with urea was used impregnate γ-alumina with a $Co(NO_3)_2 * 6H_2O$ precursor to ensure a homogeneous loading on the powder catalyst as a whole [17]. This result is harder to acquire with traditional incipient wetness impregnation [18]. Another benefit of the decomposition precipitation method over incipient wetness impregnation was that the first method could also be employed on the foam catalyst thus making the comparison between the two support types easier.

   The impregnation of the powder catalyst was achieved with the following method [17]: An aqueous solution of 1.2 M urea and precursor $Co(NO_3)_2 * 6H_2O$ is mixed in a flask while stirring. To stir the mixture the flask was placed over a magnetic stirrer which was equipped with a temperature sensor. A water-cooled reflux was placed above the flask to prevent the water from evaporating out of the flask. The amount of cobalt in the solution was 15 w% of the amount of alumina which was being impregnated, to achieve a loading of 15 w% on the catalyst.

   When the solution was made, 5 grams of alumina powder was added. After that the solution was heated to 95 ^oC. At temperatures higher than 60 ^oC urea decomposes with the presence of water resulting in the formation of metallic hydroxyl groups which easilly attach to the support and increase the pH of the solution [19]. During the impregnation the pH of the solution was measured with a digital pH meter. The impregnation was complete when the pH of the solution had a value of 7.5. The alumina was separated from the solution by decanting the solution from the alumina. After that, the alumina was washed with demineralised water and dried in an oven overnight at 120 ^oC.

3. Calcination:
   The impregnated catalyst was calcined overnight on a temperature of 400 ^oC with a temperature increase of 5 degrees per minute to decompose the precursor on the catalyst [20]. This process changed the color of the catalyst from bright pink to black indicating that the precursor had decomposed forming cobalt oxide on the catalyst surface.

4. Reduction & passivation:
   After calcination the catalyst was reduced by exposing the catalyst to a hydrogen flow. Hydrogen at room temperature was flowed with 20 cm^3/min over the catalyst with a increasing temperature of 5 degrees per minute to a maximum of 750 ^oC for six hours. At this temperature the catalyst will fully reduce. The catalyst was cooled down to room temperature in hydrogen flow and passivated by flowing a mixture of 2% O_2/He (20 cm^3/min) over the catalyst for one hour [21]. The passivition prevents rapid oxidation of the cobalt after reduction which leads to an exothermic reaction. The exothermic reaction leads to a possible fire hazard and catalyst degradation by sintering. To prevent

the exothermic reaction a small amount of oxygen is introduced which creates a small layer of oxidation on the cobalt.

2.2 Foam catalyst preparation

The preparation of foam catalysts requires a few additional steps compared to the powder catalyst. Alumina foams are initially not porous structures. A washcoat needs to be applied to ensure the adhesion of active metals on the foam [22]. Before a washcoat can be applied the foam is pretreated with $NaOH$ and anodized. This process creates a small oxide layer on the surface of the foam which increases the adhesion of the washcoat layer. The production of foam catalysts resulted three types of foams. Depending on the type a washcoat thickness of 7 μm, 17 μm and 30 μm. The following section describes the method used for the preparation of foam catalysts.

1. $NaOH$ pretreatment:
   To remove the oxide layer on the foam, the foam was placed in a 1 M $NaOH$ solution on 60 ^oC for 15 minutes. The removal of the oxide layer ensures electrical contact between the foam and clamps used in the next anodization step. After 15 minutes of contact in the $NaOH$ solution the foam was washed with demineralised water three times to ensure the removal of $NaOH$ [23].

2. Anodization:
   The foam was placed in a 10 liter water bath at room temperature containing 0.5 M of phosphoric acid and 0.08 M of oxalic acid. The foam was placed in a clamp through which the electrical current runs. A airstream was placed underneath the foam to ensure a constant temperature for the anodization. The foam was then anodized for 1 hour with a electrical current of 2.06 A and a electrical potential of 0.01 V. After anodization the foam was placed in an oven at 120 ^oC to dry overnight.[23]

3. Washcoating:
   On the anodized foam one or several washcoats were applied. The washcoat was made by mixing water 20 w% of γ-alumina and 10 w% of boehmite particles of 0.05 μm with water at a pH of 7. In the washcoat mixture the boehmite acts as a binder between the γ-alumina and the aluminium foam. A particle size of 50-0 μm γ-alumina was used and was acquired in a similar method as the powder support size. After combining all components for the washcoat, the washcoat was stabilized by mixing it for 2 hours. When the slurry was stable, the washcoat was applied by dipping the foam in the slurry for 1 minute. Excess slurry was removed with an air stream after which the foam was set to dry at room temperature. Each half hour the foam is turned around to ensure a evenly distributed washcoat. After an hour the washcoat is set and is placed in an oven at 120 ^oC overnight to remove water from the washcoat. The foam piece was weighed after drying to determine the weight of washcoat on the foam. The washcoat weight was then used to determine the loading of active metal on the washcoat. After applying

the washcoat the foam was calcinated at 600^oC to transform the boehmite to γ-alumina. A thicker washcoat was formed by repeating the washcoat methods until the wanted thickness was acquired [23]. For small additions of washcoat a thinner washcoat was applied containing 16.66 w% of γ-alumina and 8.33 w% of boehmite particles of 0.05 μm and water.

4. Impregnation and calcination:
   The impregnation and calcination steps were done in a similar method employed for the powder catalyst preparation. Figure 2.2 shows the appearance of foam pieces after specific stages in the preparation.

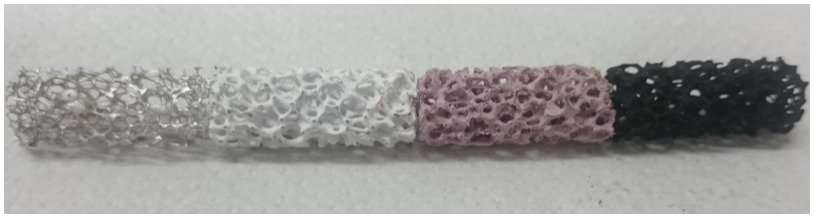

Figure 2.2: Foam pieces after it's preparation step: original, washcoating, impregnation, calcination

5. Reduction:
   It was impossible to reduce the foam catalyst with a similar method as the powder catalyst due to the melting point of the aluminum foam at 660 ^oC. As alternative the foam was reduced by using a reduction agent, $NaBH_4$. The foam was reduced submerging it a solution where 5 mols of $NaBH_4$ for every mol of cobalt on the foam was added to 20 ml of water. Subsequently the foam was placed in this solution. This resulted in hydrogen bubble formation on the surface of the foam. after 30 minutes the the bubble formation stopped and the foam catalyst was reduced. The foam was then washed with demineralised water and was directly placed in the reactor. In the reactor the foam was dried with a N_2 airstream on 120 ^oC [24].

2.3 Catalyst Characterization

After the catalysts were produced, the catalyst underwent several analyses to characterize the it. To give insight in the performance of the catalyst the particle size distribution, dispersion of the active phase, pore volume, surface area, pore diameter, structures of the active phase and loading of the catalyst were tested by employing several analysis methods. The following section describes the methods used:

1. BET:
   To find out the surface area of the prepared catalyst a BET analysis was used. The BET analysis was carried out in a Micrometrics Tristar II analyser. The prepared powder

catalyst a sample is analyzed after calcination and for foam catalyst the washcoat layer is analyzed before the washcoat is applied. The sample was flushed with nitrogen on a similar temperature of the reactor 230 ^oC. After cooling down the analysis device measured the total pore volume, surface area and pore diameter of the sample.

2. TPR:
   A TPR analysis was carried out to give an indication of oxidation states of the active phase on the catalyst. The TPR was carried out on a Micrometrics Autochem II analyzer. This machine was also used for chemisorption analysis. The powder catalyst was reduced in a hydrogen flow ramping with 10 ^oC per minute to final temperature of 850 ^oC. TPR was not performed on the foam catalysts

3. ICP:
   For the determination of the loading of the catalyst ICP is used. To determine the loading of the catalyst a sample catalyst powder of approximately 33.3 mg was weighed and dissolved in 5 ml 1:1 H_2O & H_2SO_4 The solution was heated to 150 ^oC until the cobalt and the support was dissolved. After dilution the mixture was analyzed with a Amatex Spectroblue ASX-520 to measure the loading of cobalt. For the foam catalysts a similar method was used. The quantity of the H_2O & H_2SO_4 solutions was larger (40 ml) to dissolve the aluminum structure.

4. TEM:
   To find out the particle size distribution of the active phase TEM was applied on the powder catalysts. TEM measurements were taken on a scale of 1 cm : 20 nm. TEM was not performed on the foam catalysts.

5. SEM:
   SEM was applied to measure pore sizes of the alumina foam before preparation for the calculation of the washcoat thickness of the foams. SEM measurements were taken on a scale of 1 cm : 1 mm. The washcoat thickness was calculated by using the diameter of the strut and the size of the of the catalyst. By using equation 2.1 the porosity of the foam was calculated. A new porosity was then calculated using equation 2.2 which was used to calculate the toruosity of the foam with equation 2.3. It was assumed that the pore size of the foam stayed constant. Using equation 2.4 the washcoat thickness was calculated. For this calculation it was assumed that the washcoat was equally distributed over the whole foam.

$$\epsilon_{f,old} = \frac{3d_{pore}^2 d_{strut} - 2d_{pore}^2}{d_{strut}^3} \tag{2.1}$$

$$\epsilon_{f,new} = \epsilon_{f,old} - \frac{\frac{m_{wc}}{\rho_{wc}}}{V_{foam_piece}} \tag{2.2}$$

$$\epsilon_{f,new} = \chi(\frac{3-\chi}{2})^2 \tag{2.3}$$

$$2d_{wc} = \frac{2d_p}{3-\chi} - d_{strut} \tag{2.4}$$

2.4 Catalyst activity testing

For the activity testing a packed bed reactor was used. Inside a Carbolite Gero 30-3000 oven a packed bed reactor of 10 cm in length and 1 cm diameter was present. This reactor provided a space for the catalyst to conduct the Fischer Tropsch reaction. After the packed bed, A cold- and a hot-trap were used to catch the longer solid and liquid hydrocarbons after which the remaining gaseous mixture was analyzed with a Trace 1300 Gas Chromatograph. A flow diagram of the setup is shown in figure 2.3. As internal standard nitrogen was used to account for volume changes in the reactor while the synthesis took place. While operation of the setup is in a continuous setting, the measurement of the GC is not. The GC takes a sample of the gas and measures all components in a sequence lasting 50 minutes. It is only possible to measure one sample per hour. For this reason the steady state conditions were taken into account for determination of conversion selectivity and yield of the FTS.

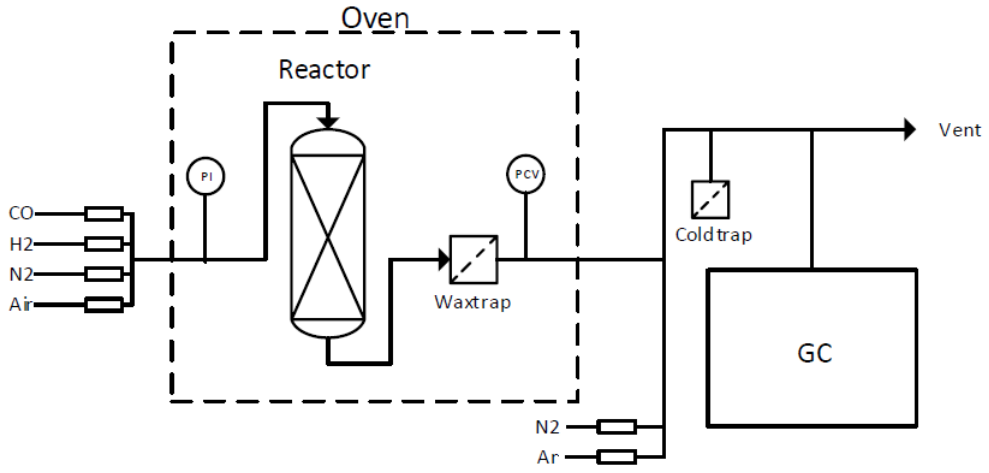

Figure 2.3: Flow sheet of the activity testing setup

In the reactor six catalysts were tested. Three powder catalysts and three different foam catalysts. All catalysts were tested on 210, 225 and 240 ^{0}C and a Weight Hourless Space Velocity (WHSV) of 36 $m^3/kg_{cat}h$. The WHSV is defined in equation 2.5. For the powder catalyst size of 50-0 μm and the foam catalyst of 17 μm WHSV of 12, 24, 36 and 48 were tested on 210, 225 and 240 ^{0}C. Hydrocarbon products up until C_{20}, CO_2, CO, H_2 and N_2 were measured with the GC. Originally the the foam catalyst of 17 μm would be tested on WHSV of 12, 24, 36 and 48, this was changed to only a WHSV of 36 due to inactivity of the foam catalysts. The

following equations show the calculations for conversion, selectivity and adjusted selectivity of the reaction.

$$WHSV = \frac{\Phi_v}{m_{cat}}[m^3/kg_{cat}h] \tag{2.5}$$

$$X_{CO} = \frac{\Phi^{CO}_{mol,in} - \Phi^{CO}_{mol,out}}{\Phi^{CO}_{mol,in}} \tag{2.6}$$

$$S_i = \frac{\Phi^{i}_{mol,out}}{\Phi^{CO}_{mol,in} - \Phi^{CO}_{mol,out}} \tag{2.7}$$

$$S' = \frac{S_i}{\sum S_p roducts} \tag{2.8}$$

Where S' is the adjusted selectivity, a selectivity over all measured products. To account for the production wax, which is not measured by the GC the wax-traps and the catalysts were checked for wax formation.

- TGA:
  After activity testing the catalyst the both wax-traps were checked for wax by weighing the wax traps before and after cleaning them. TGA was used check the wax content in the the powder catalysts. Where 20 mg of powder catalyst was heated to 750 ^{o}C with a heating rate of 5 ^{o}C/min in a TGA/DCS 1 Star^e system. The foam catalysts were placed in an oven overnight at 120 ^{o}C to remove any water in the catalyst. Subsequently the foam was weighed and calcined at 500 ^{o}C for 8 hours with a heating rate of 10 ^{o}C and weighed again.

Chapter 3

Numerical model

A mathematical model of the FTS has been made. The purpose of the model was to compare experimental results with results from the model to indicate if the acquired experimental results are in agreement with known kinetics. This section describes equations used for the modeling of the reactor.

In order to model the FTS two models were made; a particle model and a reactor model. The reactor models an PBR filled with a foam or powder catalyst. The model solves the concentration of bulk gasses over the length of the PBR. On each length position of the reactor the particle model solves the reaction which takes place in the internal volume of the particles. The balance for the reactor model is shown in equation 3.1. The reactor is modeled as a isothermal reactor.

$$\frac{(dC_i^{bulk}\Phi_v)}{dz} = \frac{dF_i^{bulk}}{dz} = A_{0,r}a_{gs}k_{gs}(C_i^s - C_i^{bulk}) \tag{3.1}$$

Where:

$$F_{tot} = \sum F_i \tag{3.2}$$

$$P_i = \frac{F_i}{F_{tot}}P_{tot} \tag{3.3}$$

It is assumed that the pressure is constant over the whole reactor. The ideal gas law is be used to calculate the bulk concentrations:

$$C_i^{bulk} = \frac{P_i}{RT} \tag{3.4}$$

The external surface area of the powder catalyst and foam catalyst needs to be specified to make the model applicable to both foam and powder catalyst. For foam catalysts the surface area is dependent of the ppi, the shape of the foam ligaments and washcoat thickness on the foam. The surface area for 20 ppi foam supports was taken from technical data of the metallic foam. The surface area of 20 ppi foam support is 1400 m^2/m^3_{foam}. It is assumed that the

washcoat thickness has no influence on the surface area of the foam. To model a single foam piece the total reactor length of 0.02 m is used which is the length of a single foam piece. For powder catalysts the surface area calculated as:

$$a_{gs} = \frac{6\epsilon_s}{d_p}\epsilon_{cat,bed} \quad [\frac{m_i^2}{m_s^3}] \tag{3.5}$$

Where $\epsilon_{cat,bed}$ is the fraction of catalyst in the packed bed. External mass transfer is calculated by using the correlation by Thoenes & Kramer [25].

$$Sh' = 1.0(Re')^{1/2}Sc^{1/3} = \frac{k_{gs}d_p}{D_{AB}} \tag{3.6}$$

The equations 3.7 and 3.8 show the alternative Reynolds and Sherwood numbers for different shape's of catalysts and differences in packing of the PBR. Where ϵ_s is the solid fraction in the reactor.

$$Re' = \frac{Re}{\epsilon_s\gamma} \tag{3.7}$$

$$Sh' = \frac{Sh * (1-\epsilon_s)}{(\epsilon_s)\gamma} \tag{3.8}$$

Bulk diffusion of syngas needs to be calculated in order to calculate fluxes going inward in the catalyst. It is assumed that product formation has a small effect on the external diffusion behavior of the system. Therefore the physical properties of syngas are constant and are mixed value's of H_2 and CO in the ratio 2:1. The diffusion of bulk syngas as a function of temperature and pressure is calculated by using equation 3.9 [26]:

$$D_{AB}(P_2,T_2) = D_{AB}(P_1,T_1)\frac{P_1}{P_2}(\frac{T_2}{T_1})^{1.75} \tag{3.9}$$

A particle model was made to define the reaction in the particle. The balance for the particle model is shown in equations 3.10.

$$\frac{\partial C_{i,s}}{\partial t} = -D_i^{eff}\frac{\partial^2 C_{i,s}}{\partial x^2} - \nu_i R_{fts} \tag{3.10}$$

The balances have the following boundary conditions:

$$x = 0, \quad \frac{\partial C_{i,s}}{\partial x} = 0 \tag{3.11}$$

$$x = 1, \quad D_i^{eff}\frac{\partial C_{i,s}}{\partial x} = k_{gs}(C_{i,s} - C_{i,bulk}) \tag{3.12}$$

The initial conditions for these balances are:

$$t = 0, \quad Ci, s = 0 \tag{3.13}$$

The reaction rate of the particle model if shown in equation 3.14:

$$R_{fts} = r_{fts}\rho_{cat}\frac{\epsilon_{cat,bed}\epsilon_s}{\epsilon_g}[\frac{mol}{}m_g^3 s] \tag{3.14}$$

Where r_{fts} is the kinetic expression by Yates & Scatterfield [27]. The Yates & Scatterfield kinetics are a Langmuir Hinshelwood type kinetics and is shown in equation 3.15. Where a and b are temperature dependencies of the reaction.

$$r_{fts} = \frac{aP_{CO}P_{H2}}{(1+bP_{CO})^2} \quad [\frac{mol}{kg_{cat}s}] \tag{3.15}$$

$$a = 0.1328exp[4494.41(\frac{1}{493.15} - \frac{1}{T})] \quad [\frac{mol}{kg_{cat}/bar^2 s}] \tag{3.16}$$

$$b = 2.226expe^{([-8236(\frac{1}{493.15}-\frac{1}{T})])} \quad [bar^{-1}] \tag{3.17}$$

To model the selectivity of the reaction an ASF distribution is used by Vervloet et al and is shown in equation 3.18 [2]. From the value of α of equation 3.18 the selectivity of each product is calculated using equation 3.19.

$$\alpha = \frac{1}{1 + k_\alpha(\frac{C_{H2}}{C_{CO}})^\beta exp(\frac{\Delta E_\alpha}{R}(\frac{1}{493.15} - \frac{1}{T})} \tag{3.18}$$

$$S_i = i(1-\alpha)^2\alpha^{i-1} \tag{3.19}$$

It is assumed that there is only formation of olefins with a maximal chain length of 20 and that there is no CO_2 formation. With these assumptions the stochiometry for CO, H_2 and H_2O can be calculated as followed:

$$\nu_{CO} = \nu_{H2O} = \sum_{n=1}^{20} S_i * n \tag{3.20}$$

$$\nu_{H2} = \sum_{n=1}^{20} S_i(1+2n) \tag{3.21}$$

Diffusional behaviour is different inside the catalyst particle. To model intra-particle diffusion the assumption was made that the particles are filled with wax products at t = 0. As a result

the used diffusion coefficient in the particle are the diffusion coefficients in wax media. For CO and H_2 correlations for the diffusion coefficient in wax were used [5]. For the other components reference values were used.

$$D_{CO,wax} = 5.584 * 10^{-7} exp(\frac{-1786.29}{T}) \tag{3.22}$$

$$D_{H2,wax} = 1.085 * 10^{-6} exp(\frac{-1624.63}{T}) \tag{3.23}$$

The effective diffusivity is a function of catalyst parameters as well. Using reference values for catalyst porosity and tortuosity the effective diffusivity is calculated as followed:

$$D_i^{eff} = D_{i,wax} \frac{\epsilon}{\tau} \tag{3.24}$$

The model was used under similar conditions as the reactor of the activity testing. To evaluate the differences between modeling results and experimental results powders with a size of 100 μm (P3), 75μm (P4) and 50 μm (P5) and foam catalysts size of 30 μm (F1), 17 μm (F2) and 7 μm (F3) were modeled on a temperatures of 210, 225 and 240 ^{0}C and WHSV of 36 $m^3/kg_{cat}h$. The foam size of 17 μm and powder size of 50 μm were modeled with a range of WHSV 12, 24, 36 and 48 $m^3/kg_{cat}h$ on temperatures of 210, 225 and 240 ^{0}C.

Chapter 4

Results and Discussion

4.1 Catalyst characterization

Sizing of the catalyst support

- Powder:
  The powder support was prepared by pelletizing and crushing for which the method was described in the catalyst preparation section. This resulted in five support fractions of 150-125, 125-100 ,100-75 ,75-50 and 50-0 μm.

- Foam:
  In order to evaluate the thickness of the metallic foam strut SEM measurements were made. Figure 4.1 shows the result of the SEM measurements before and after applying the washcoat.

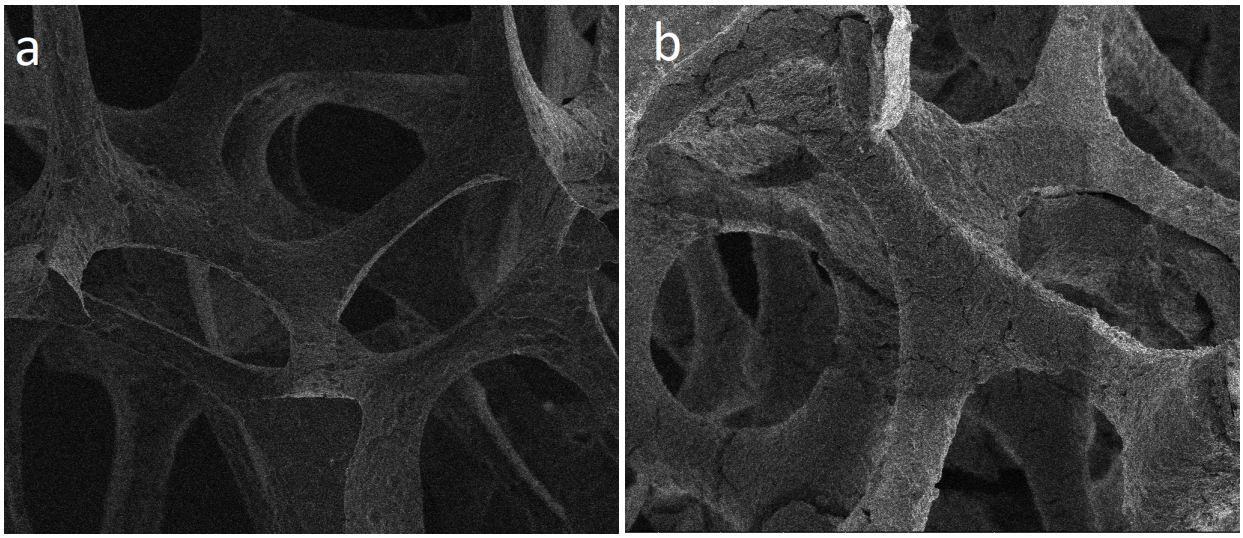

Figure 4.1: a: SEM image of foam structure, b: Foam structure after a applied washcoat

SEM images show a complete coverage of the foam surface by a well adhered alumina washcoat, in agreement with simple visual observations. The thickness of this alumina layer could not be determined from the SEM images because all visible struts were fully covered. Therefore, the washcoat thickness was indirectly determined by calculations described in equations 2.1-2.2. Using the weight of the applied washcoat, the thickness of the foam strut and poresize of the foam the washcoat thickness was determined [28]. Three groups of foams with different washcoat thicknesses were made with a washcoat thickness of 7, 17 and 30 μm.

Specific Surface Area and Pore Size Distribution

Previous studies have shown that active phase sizes of 8 nm is ideal for optimal FTS activity. The effect of cobalt particle size on the effectivity of the catalyst is grafically shown in Figure 4.2 [29].

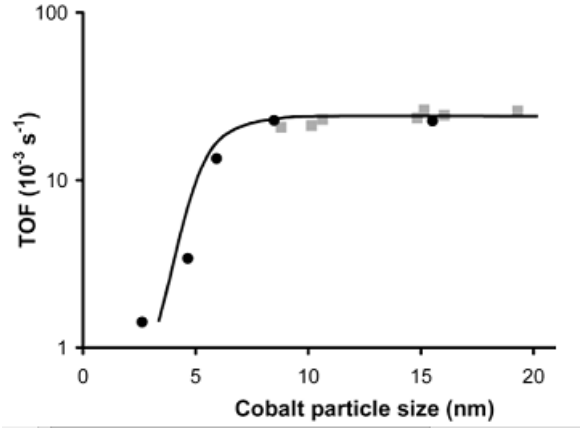

Figure 4.2: Effect of Cobalt size on FTS

Figure 4.2 shows that a minimal cobalt size of 4 nm is required to have activity in FTS. From a cobalt particle size of 8 nm an increase in particle size does not increase the FTS activity of the catalyst. The pore size, pore volume and surface area of the catalysts were determined by nitrogen physisorption. The following figure shows the results of the BET measurements which were used to determine the poresize and internal volume of the different sized powder catalysts.

- Powder:
  Figure 4.3 shows the results for the BET measurement carried out on the powder catalysts.

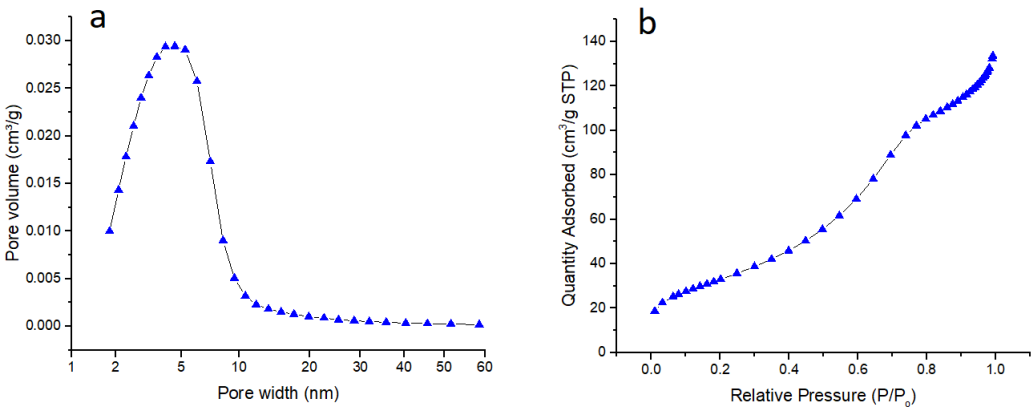

Figure 4.3: a: Pore size distribution of 150-125 μm catalyst, b: Adsorption isotherm of 150-125 μm catalyst

The adsorption isotherm and pore size plots show similar results for all powder catalysts. The poresize distribution shows a large volume for pores with a pore width around 5 nm. This indicates that it is possible to acquire cobalt particles with a sufficient size for FTS activity. Results for BET measurements on all powder catalysts are shown in Table 4.1
By pelletizing and crushing the alumina support a decrease in pore volume and pore size is expected this is due to the collapsing of larger pores. Pelletizing and crushing the support has no influence on the internal surface area. The results of BET measurements on the powder catalysts show the described effects for the poresize and surface area. For the pore volume no clear effect of pelletizing is observed.

- Foam:
  It was not possible to perform BET measurements on the coated foam catalysts. As comparison a BET measurements were carried out on a washcoat sample, which was obtained by producing the washcoat similar to the applied washcoat and drying it. The measurements of washcoat was analogous to the powder BET measurements. The poresize distribution and adsorption isotherm of the washcoat are shown in Figure 4.4.

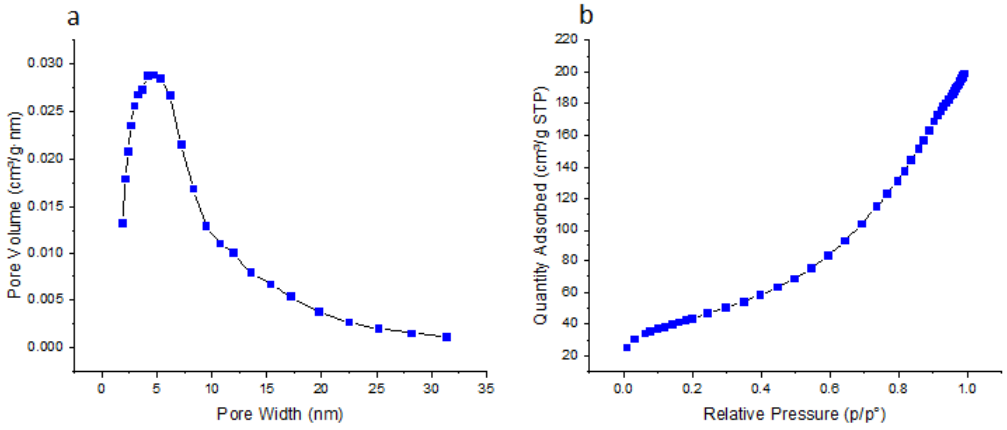

Figure 4.4: a: Poresize distribution of washcoat b: Adsorption isotherm of washcoat

Comparison of the BET results for the washcoat and powder catalysts shows that the pore size distribution for the washcoat is larger then for the powder catalyst samples. There is a lot more volume adsorbed for pore sizes of 10-15 nm for the washcoat sample. Due to the larger pore size the catalyst should be able to contain larger cobalt particles which are beneficial for the activity of the catalyst. The total adsorbed volume and surface area of the washcoat is larger compared to the powder support. This is due to the presence of boehmite binder in the washcoat mixture. Results for BET measurements on the washcoat is shown in table 4.1.

Catalyst size μm	V_{pore} (cm^3/g)	$d_{pore}(nm)$	$A(m^2/g)$	mean Cobalt particle size (nm)
150-125	0.212028	5.5017	119.850	2.6266 ± 0.1522
125-100	0.212482	5.5687	120.276	4.6077 ± 0.2873
100-75	0.245544	5.9227	131.931	4.5406 ± 0.2908
75-50	0.228098	5.4152	135.472	4.4551 ± 0.2188
50-0	0.233653	5.3073	138.423	4.1785 ± 0.3580
Foam, 50-0 μm	0.315519	7.7111	143.423	-

Table 4.1: Results BET and TEM measurements

Size of cobalt particles

- Powder:
  A result of a TEM measurement is shown in figure 4.5. From these images the particle size distribution of cobalt on the catalyst was made. The results of the particle size distribution is shown in the table 4.1. The following figure shows the cobalt particle size distribution of for the 100-75 μm powder catalyst.

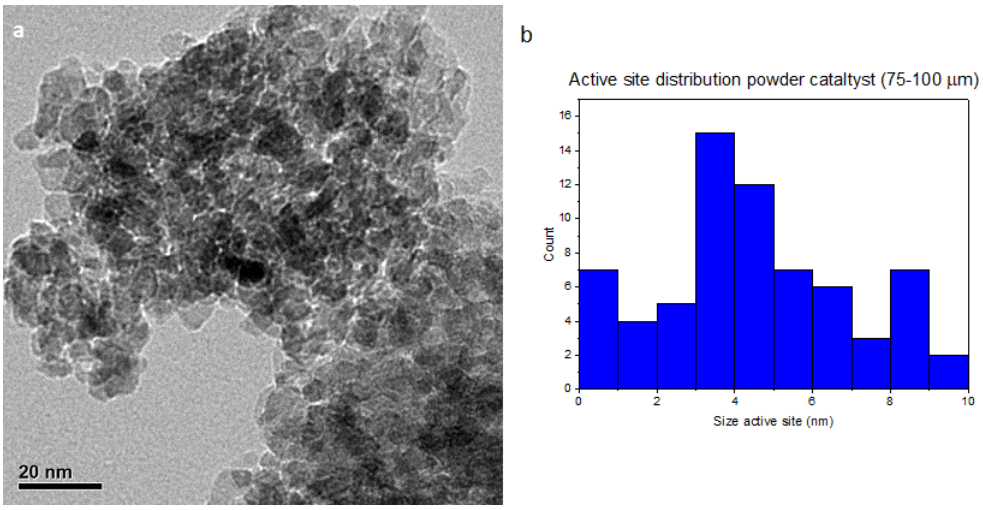

Figure 4.5: a: TEM image catalyst, b: Particle size distribution

From the TEM measurements a mean cobalt particle size of 4 - 4.6 was found on most

of the powder catalysts. The largest powder support shows a smaller particle size on the catalyst compared to the others. This result cannot be explained by BET results. Why the largest powder support contains smaller cobalt particles is unknown. Between 125-100 and 50-0 μm a decrease in cobalt particle size with decreasing catalyst particle size and average pore size can be seen. It is known that the size of the active phase is influenced by the pore diameter of the support. The decrease in cobalt particle size follows a different trend as the previously seen BET pore diameter results. The cobalt particle size for the powder catalysts is large enough to present FTS activity, with the exception of the 150-125 μm catalyst. Based on Figure 4.2 the 150-125 μm catalyst is most likely not active since this catalyst has a small cobalt particle size of 2.6 nm.

- Foam:
  TEM measurements on foam catalysts were not taken.

Oxidation states of cobalt

- Powder:
  TPR measurements on the powder catalysts show a similar result for all catalysts. Figure 4.6 shows the TPR plot of the 150-125 μm catalyst.

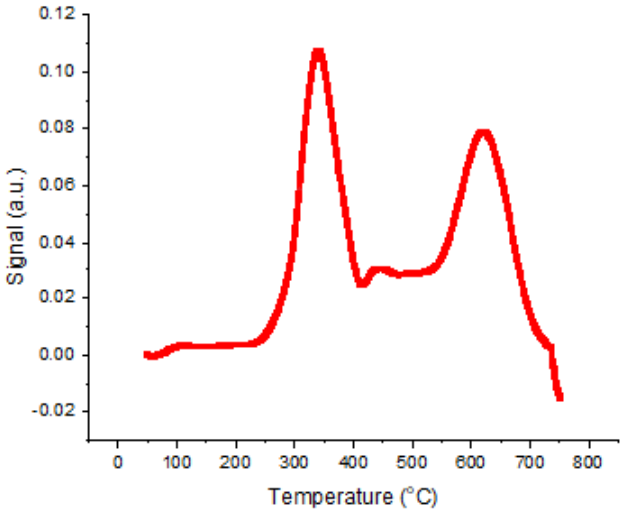

Figure 4.6: TPR plot of powder catalyst P1

The TPR result in figure 4.6 shows two peaks. These indicate the reduction of Co_3O_4 to CoO and the reduction of CoO to $Co(0)$. The results of the TPR measurements on powder catalysts are shown in Table4.2. The temperature of reduction is influenced by the size of the support and the size of the active phase. Small cobalt particles are harder to reduce due to a larger interaction with the support, leading to an increase in reduction temperature. The size of the support influences the reduction temperature due to intra-particle diffusion of H_2. In larger support catalyst particles would take longer to re-

duce, which leads to higher reduction temperatures due to the set temperature program. Comparing BET results, size of the cobalt particles and the reduction temperatures of the catalysts give no explanation for the differences in reduction temperatures. Due to the combining effect of the two opposite effects of cobalt particle size and diffusion path no clear trend was found in reduction temperatures.

Catalyst size (μm)	Cobalt particle size (nm)	1st peak temperature (^oC)	2nd peak temperature (^oC)
150-125	2.62	340.3	620.4
125-100	4.61	380.3	737.5
100-75	4.54	306.2	615.8
75-50	4.46	328.1	700.1
50-0	4.18	336.5	705.8

Table 4.2: Results TPR characterization

- Foam: No TPR measurements were carried out on the foam catalyst.

Loading of the catalyst

The loading of the catalysts was acquired by ICP measurements. All catalysts were made to have an loading of 15 w% of cobalt on the support. ICP results show that all catalysts have a loading of approximately 15 w%. For two foam catalysts the loading was slightly lower. Results are shown in the following table:

Catalyst label	Catalyst size (μm)	loading (w%)
P1	150-125	15.1
P2	125-100	15.0
P3	100-75	15.0
P4	75-50	14.9
P5	50-0	15.0
F1	30	14.1
F2	17	15.0
F3	7	14.1

Table 4.3: Results ICP characterization

4.2 Activity tests on powder catalysts

Activity tests were carried out on the catalysts. The results of the foam catalysts and 100-75, 75-50 and 50-0 μm powder catalysts are shown in this section. While the reaction was carried out, a sample of the gas from the reactor was analyzed in the GC to measure the composition of the gas. When the conversion of CO was equal for three consecutive samples the reactor

was at steady state After achieving steady state the last measurement was used to calculate the conversion and selectivity for each product.

The activity tests on the 150-125 μm catalyst showed that there is indeed no FTS activity for this catalyst. The other powder catalysts have a larger particle size, compared to Figure 4.2 the powder catalysts have a sufficient cobalt size for activity but the activity could be much larger if larger cobalt sizes were obtained. Results for the 125-100 μm catalysts were not obtained due to time constraints.

Effect of residence time on performance powder catalyst

The smallest catalyst (50-0 μm) was tested at multiple temperatures and flowrates. The conversions for the test on the 50-0 μm catalyst are shown in figure 4.7-a.

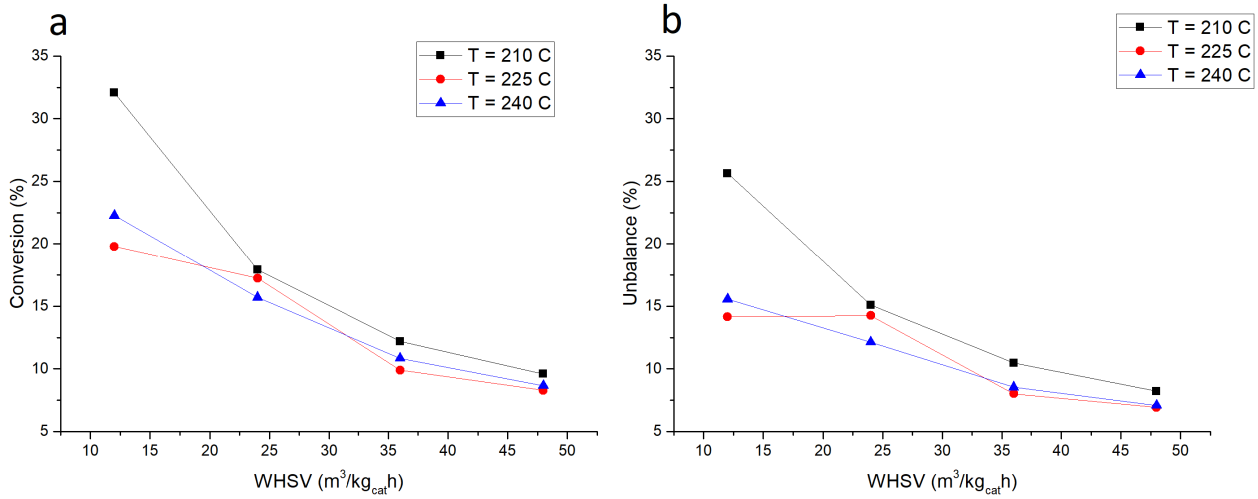

Figure 4.7: a: Effect of WHSV on conversion of CO for catalyst P5 on 2 MPa at temperatures of 210, 225 and 240 ^{0}C. b: Unbalance of the measurements for catalyst P5

Figure 4.7-a shows that the conversion of the reaction decreases by increasing flow rate in the reactor. A decrease in flow rate under similar reactor conditions leads to an increase in space time within the reactor. As a result the conversion of CO increases. Figure 4.7-b shows that the carbon balance does not close for the measurements. The shape of the unbalance resembles the shape of the conversion. This shows that only a small amount of product is detected in the measurements.

The large unbalance could be due to the formation of wax products which stay on the catalyst surface or in the inert γ-alumina filling in the reactor which are then not measured. Another possible cause of the unbalance is a leak in the reactor before the feed gets into contact with the catalyst. This would decrease the amount of CO compared to the internal standard, resulting in an increased CO conversion. This is not likely since the setup has CO detection in case of a leak.

Figure 4.10 shows the effect of particle size, temperature and flow rate on the selectivity of the

FTS. The effect of an increase in flow rate on the selectivity shows an increase in selectivity for smaller product formations. The selectivity to $C10 - C14$ products a decreases when the flow rate is increased. From these results it can be concluded that the chain growth is decreased with increasing flow rates. Lower flow rates represent a longer residence time. Chain growth increases when increasing the residence time, which is line with a mechanism in which $-CH_2-$ groups are sequentially added to the growing chain as the reaction proceeds. At first, smaller hydrocarbons are formed, and therefore H_2 is consumed faster than CO, lowering the H_2/CO ratio, and thus promoting longer hydrocarbon formation at longer residence times.

Effect of temperature on performance powder catalyst

The effect of temperature on the conversion of the powder catalyst is shown in the following figure:

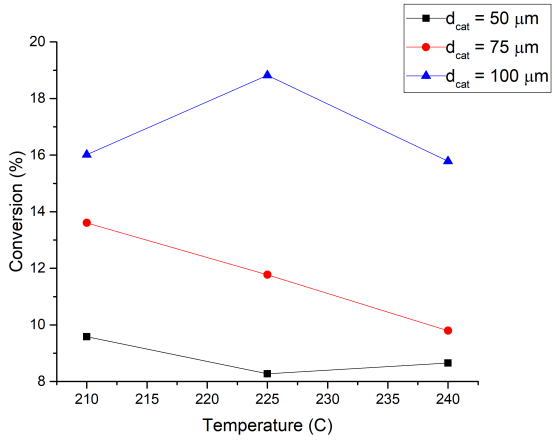

Figure 4.8: Conversion as a function of temperature for different powder catalysts on a pressure of 20 MPa and WHSV of 36 $m3/kg_{cat}h$.

Figure 4.8 shows that the conversion of the FTS decreases with increasing temperature. A possible reason for the decrease in conversion could be external diffusion limitations. If there were no external limitations the conversion should increase due to an increase in reaction rate. To check if there are any external diffusion limitations the Carberry number is evaluated: [30]

$$Ca = \frac{r_{obs}}{a_{gs}k_{gs}c_{bed}} < \frac{0.05}{|n|} \tag{4.1}$$

Where n is the order of the reaction and is assumed for this calculation to be equal to 1. The reaction rate is defined as the amount of mole CO consumed in $[kmol/kg_{cat}s]$.

The calculation of the Carberry number is shown in the appendix and has a value of: 0.0055. The Carberry number shows that the effect of external mass transfer can be neglected. A large portion of the conversion is due to CO_2 formation by the water gas shift (WGS) reaction.

This shows that the catalyst is primarily active for the WGS reaction in stead of FTS. A large decrease in CO_2 selectivity with increasing temperatures can be observed in Figure4.10. To give insight in the amount of product produced molar flows of hydrocarbon products and CO_2 is shown in figure 4.9.

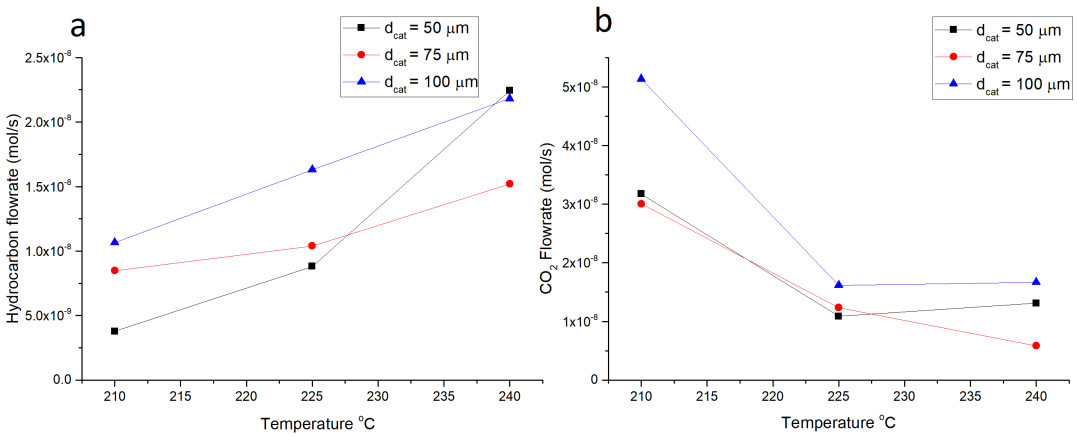

Figure 4.9: Molar flows of hydrocarbons and CO_2 of activity tests

Figure 4.9-b shows a decrease for CO_2 productivity with an increasing temperature. This is in agreement with thermodynamics of the WGS reaction which is unfavourable at higher temperatures. Therefore, the production of CO_2 should decrease with an increase in temperature. Figure 4.8 shows a decrease in conversion of CO with increasing temperatures. By comparing molar flow rates from Figure 4.9 it is seen that the amount of CO_2 formation is quite large compared to hydrocarbon formation. This suggests that the formation of CO_2 has a larger contribution to the conversion than the FTS. It is observed that the FTS activity increases with increasing temperature. Comparing the trends in FTS with WGS activity shows that the decrease in WGS activity does not increase the activity for FTS. This shows that the reactions occur simultaneous with no competition between the two reactions.

Figure 4.10-b, c & d show a large decrease in CO_2 selectivity for all catalysts at higher temperatures. The graphs also show an increase in selectivity of all hydrocarbon products at higher temperatures. The larger selectivity of hydrocarbons is partially due to the decrease of CO_2. The increase in methane is according to literature. The increase in the $C5-C9$ and $C15+$ products is due to a smaller chain growth probability, leading to a reduction in immeasurable wax formation and an increase in shorter measurable products which mostly consists of large $C5+$ products. An increase of the operating temperature leads to a an increase in the production of hydrocarbons with an increase in selectivity for shorter hydrocarbons.

Effect of particle size on performance powder catalyst

From Figure 4.8 it can be seen that an increase in catalyst size shows an increase in CO conversion. This contradicts the possibility of external diffusion limitations, since an increase of particle size decreases the surface area of the particle and thus the external mass transfer.

The higher conversion for larger catalysts could be due to a more active catalyst in WGS of the larger particles seen in Figure 4.9-b.

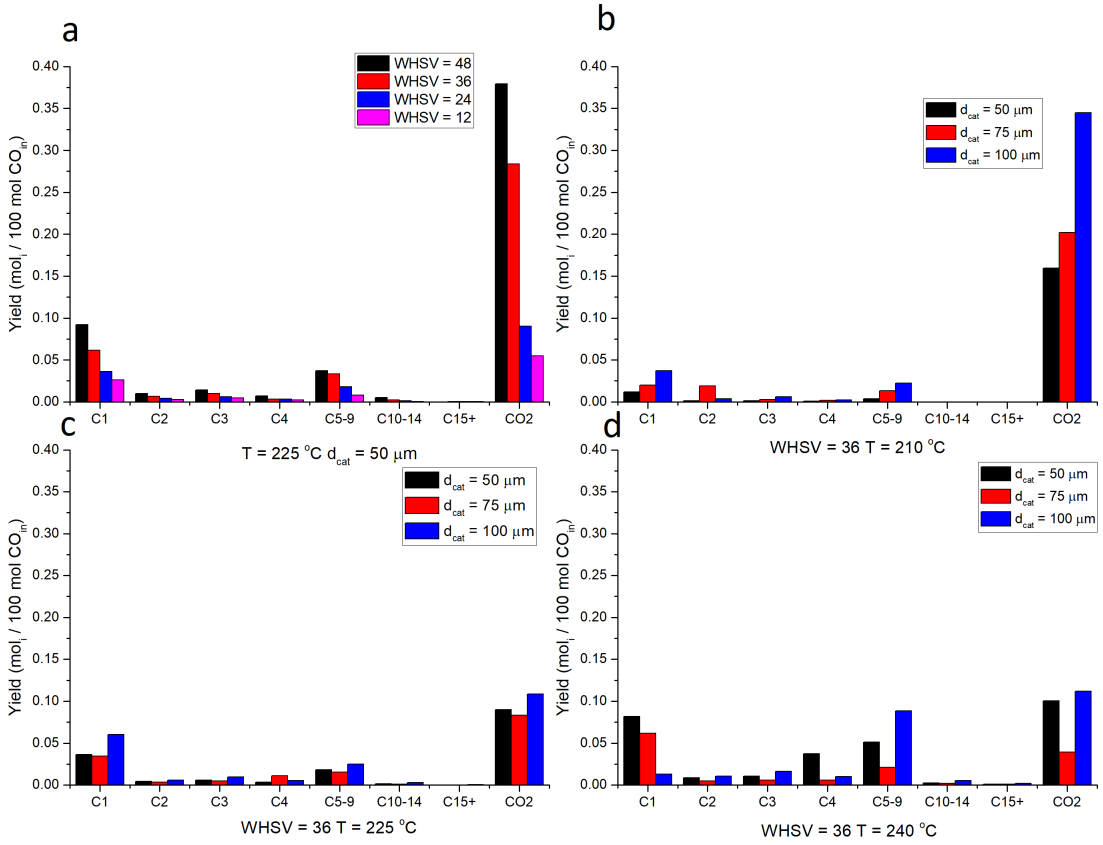

Figure 4.10: Selectivity effects on experimental results of a: Catalyst size on T = 210 ^oC, b: Catalyst size on T = 225 ^oC, c: Catalyst size on T = 240 ^oC ,d: Flow rate on 50 μm catalyst

The measurements show small differences in selectivity between catalyst sizes. At 210 ^oC and 225 ^oC an increase in small hydrocarbons is observed when the particle size is increased. This effect is due to differences in catalyst activity previously shown in Figure 4.9-a. At 240 ^oC the conversion of the 50 and 100 μm are roughly similar. The selectivity plots show a difference in selectivity for these catalysts. The smallest catalyst shows a higher yield in methane formation compared to the largest catalyst. For longer hydrocarbon chains the largest catalyst has a higher yield. This result is the opposite of what would be expected if diffusion limitations occur. Therefore, it is concluded that diffusion limitations are absent for the powder catalysts. Most likely this is due to the low amount of catalyst activity which leads to a kinetically limited system instead of limitations due to intra-particle diffusion. Larger effects in selectivity may be observed if a larger quantity of products was measured.

The amount of wax formation was not used in the selectivity calculations since it is unknown what the rate of wax formation is different reaction conditions like flowrate, temperature reaction start up. The following graph shows the result of TGA measurements made after the activity tests:

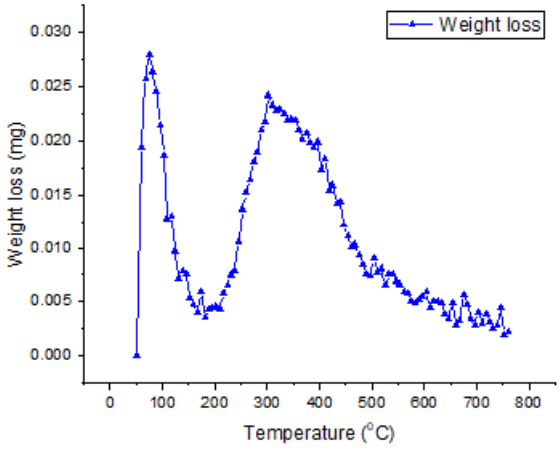

Figure 4.11: TGA plot on powder catalyst P4 after reaction

Figure 4.11 shows the results of the TGA measurement on the catalyst after activity testing. In the graph two peaks are seen. The first peak is weight loss due to water removal. The second peak shows the removal of hydrocarbon components. By taking the area of the peak a weight percentage of product on the catalyst can be calculated. For powder catalysts approximately 2 w% of the packed bed was filled with wax hydrocarbon products. The selectivity of the powder catalysts is mostly to wax products and CO_2. These products do not account for the whole unbalance of the reactor. The amount of measurable waxes do not account for the entire carbon loss, the reason of which remains an open question. Further investigation on this matter should be addressed in the future, including the (un)reliability of the gas phase analysis as a possible reason for the carbon unbalance. In the end powder catalysts with a low activity were made which selectivity is largely influenced by the WGS reaction. The low activity is most likely due to a lack of sufficiently sized cobalt active sites. Due to the low activity no intra-particle diffusion limitations where obtained.

4.3 Activity tests on foam catalysts

For activity testing on the foam catalyst three foam catalyst were tested on with a WHSV of 36 $m^3/kg_{cat}h$ and temperatures of 210, 225, 240 ^oC. Due to their insufficient catalytic activity, the foam catalysts were tested only under a limited set of conditions. All foam catalysts were tested on a WHSV of 36 $m^3/kg_{cat}h$ on 210, 225 and 240 ^oC. The following graph shows the results of the activity testing of foam catalysts:

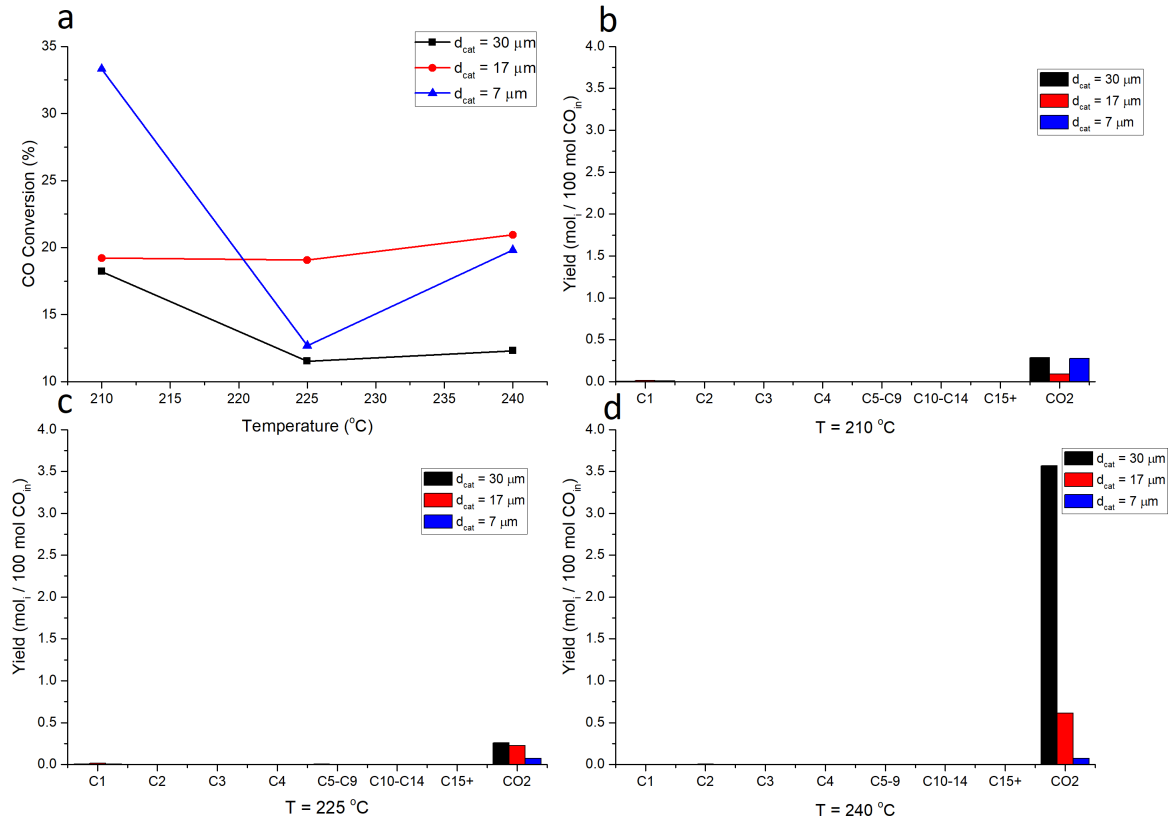

Figure 4.12: Activity testing on the foam catalysts. a: Conversion, b: Selectivity on 210 ^oC, c: Selectivity on 225 ^oC, d: Selectivity on 240 ^oC

From these results it is seen that there there is a minimal amount of product formation. All measurements show a high yield of CO_2 compared to other products. Most likely the WGS reaction fully takes over any measurable FTS activity. All foam catalyst show a large conversion of CO where the unbalance of the reaction is in all cases equal to the obtained conversion. Table 4.4 shows the wax content of the catalysts after activity tests. From these measurements it is clear that the there is a large formation of wax on the foam catalyst.

Catalyst label	Catalyst size (μm)	Wax on catalyst (w%)
F1	30	11.85
F2	17	6.19
F3	7	4.39

Table 4.4: Results wax on foam catalyst

Activity tests on foam catalysts show that there is conversion of CO in the reactor. The conversion of CO did not result in the significant formation of hydrocarbons. While small amounts of light hydrocarbons were measured, a larger quantity of CO_2 was measured. Measurements taken in the transient part of the reaction showed no CO or H_2 peaks suggesting consumption of reactants. Most likely the foam was active at the start of the reaction on steady state the FTS on foam catalyst was absent due to the high WGS activity of the reaction. The initial product

formation on the catalyst surface could have caused the catalyst to deactivate with only activity WGS reaction remaining. From the WGS activity it can be seen that the selectivity toward CO_2 is increased if the washcoat thickness is increased.

Incomplete reduction of the catalyst has been consider as possible cause of low catalytic activity of the foam catalysts, as they were reduced at a slightly lower temperature (600 ^oC) to prevent melting of the foam structure. Alternatively, both foam and powder catalyst were reduced in liquid phase with $NaBH_4$ and similar results were obtained. Thus, it is concluded that incomplete reduction of the cobalt in the case of the foam catalyst is not a likely cause for its low activity.

Finally, we may also attribute the low FTS activity of the foam catalyst to the washcoating procedure. The color change in the different steps of the catalyst preparation and the ICP measurements show that the aimed cobalt loading was acquired. However, the size of the cobalt active phase is unknown. The size of the cobalt active phase was not measured due to size implications of the foam. BET measurements show that the pore size distribution of the washcoat do not restrict the formation of cobalt particles larger then 4 nm. The precise reason for the low activity remains unknown.

4.4 Modeling of FTS

The high unbalance in the results of the activity tests gives poor insight in diffusion limitation for FTS. Modeling of the reactor containing foams or powder catalysts under similar conditions as the activity tests could give an insight in what results should be expected if the wanted activity was acquired without CO_2 formation. Activity of the FTS was corrected for the amount of active catalyst in the reactor to achieve similar conversions to the activity tests.

Modeled activity tests for foam catalysts

The conversion for the modeled foam catalysts are shown in figure 4.13-a. It is clearly seen that the effect of temperature on the conversion does not resemble the experimental results and shows an increase in activity for higher temperatures. The experimental results showed an decrease in conversion on higher temperatures. The difference between the results due to the absence of WGS reaction.

The modeled effect of flow rate on the conversion shows that the conversion of foam catalysts has a similar shape compared to the experimental results. The effect of flow rate on the conversion is much higher compared to experimental results. This is due to the absence of WGS reaction and the larger FTS activity of the model. Results of activity tests on powder catalysts showed that the selectivity to CO_2 of the reaction is increased if the flow rate is decreased. At longer residence times (i.e., lower flow rates), the FTS becomes more significant and consequently hydrocarbon formation is evidenced.

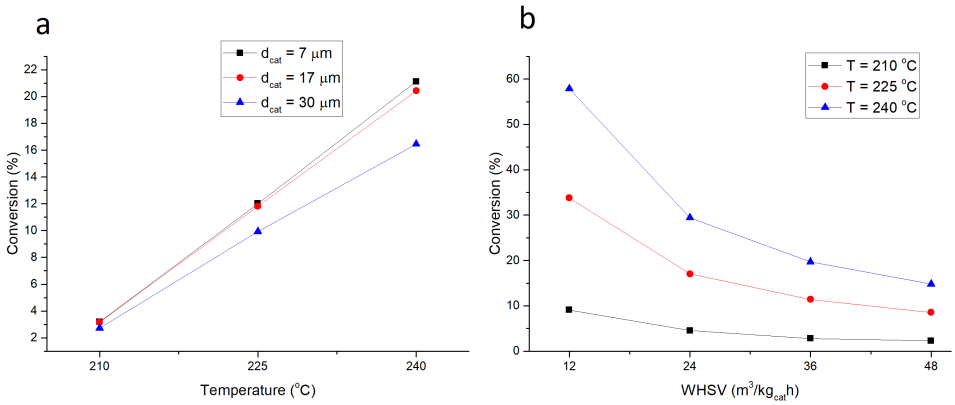

Figure 4.13: a: Effect of temperature on conversion on WHSV of 36 $[mol/kg_{cat}h]$, b: Influence of flow rate on conversion of 17 μm foam catalyst

It is also observed in Figure 4.13-a that the larger catalyst have a smaller increase in conversion on higher temperatures. The lower conversion is due to intra-particle diffusion limitations [30]. These diffusion limitations are emphasized on higher temperatures. These diffusion limitation have an influence on the selectivity as well. The following figure shows the effect of temperature, catalyst size and flow rate on the selectivity of the modeled FTS:

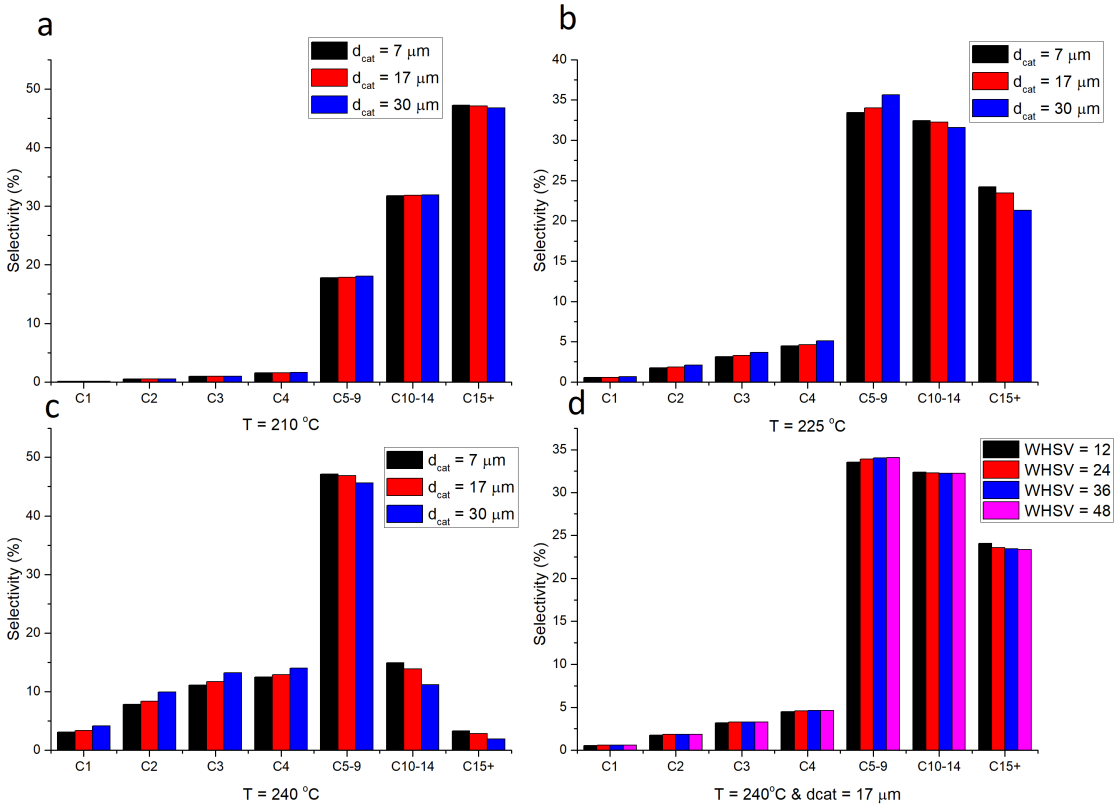

Figure 4.14: a: Effect diffusion length on FTS selectivity of foam catalysts on 210 ^oC b: 225 ^oC, c: 240 ^oC, Effect of flow rate on FTS selectivity for 17 μm foam catalysts

Figure 4.14-a shows no effect of diffusion length on the selectivity this is logical since a dif-

ference in conversion was not observed on 210 ^oC. At higher temperatures small effects of diffusion limitations are observed. The diffusion limitations increase the production of $C1$-$C4$ components and decrease production of larger hydrocarbons. The change in selectivity due to diffusion limitations is large on higher temperatures, similar to the conversion.

The largest differences in selectivity are observed between the different temperatures and not in particle size differences. It is observed that the formation of smaller hydrocarbon chains is increased with an increase in temperature, while on lower temperatures the selectivity towards larger hydrocarbons is higher. When comparing the results of the model on 240 ^oC with the results acquired in the activity tests a similar high selectivity to $C5$-$C9$ products is seen. From these results it can be concluded that the FTS on powder catalysts shares similar results to the modeled ASF distribution.

The effect of flow rate on the selectivity is shown in figure 4.14-d which shows a very slight increase in selectivity of larger hydrocarbon products at a lower flow rate. This effect is due to changes in bulk concentrations over the reactor. The H_2/CO ratio drops along the reactor due to a larger consumption of H_2 compared to CO, this effect increases with a lower flow rate due to the higher conversion in the reactor.

Modeled activity tests for powder catalysts

Powder catalysts were modeled as well to give insight in the differences between the two catalyst types. Conversion plots similar to figure 4.13 for powder catalysts are shown in the following figure:

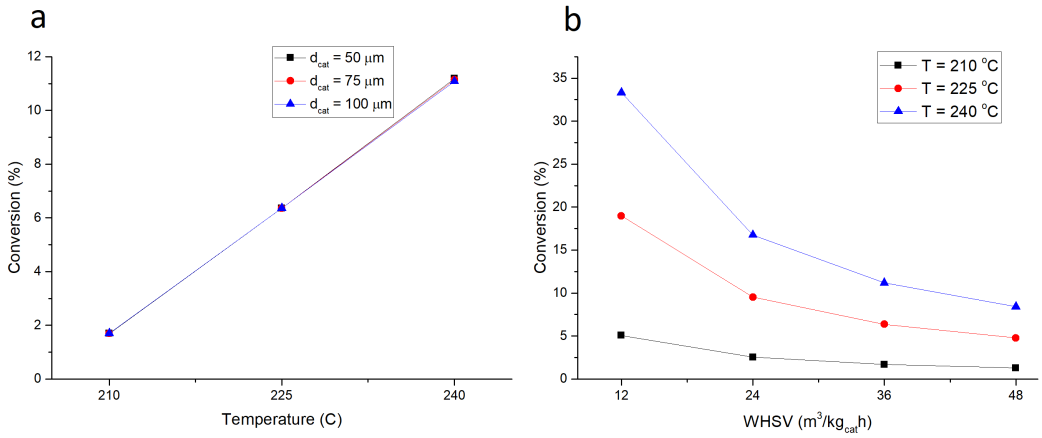

Figure 4.15: a: Effect of temperature on conversion, b: Influence of flow rate on conversion of 50 μm powder catalyst

Figure 4.15-a shows an equal conversions for different catalyst sizes on each temperature. Based on this graph there are no diffusion limitations observed in the modeling of powder catalysts. The simulations performed at various flow rates shows similar results that were observed for the to foam catalysts. The larger increase in FTS activity on lower flow rates is due to the absence of WGS in the simulation. Figure-4.16 shows the effect of flow rate, temperature

and particle size on the selectivity of FTS on powder catalysts. While the conversion plot shows no sign of intra-particle diffusion limitations the selectivity could still be affected.

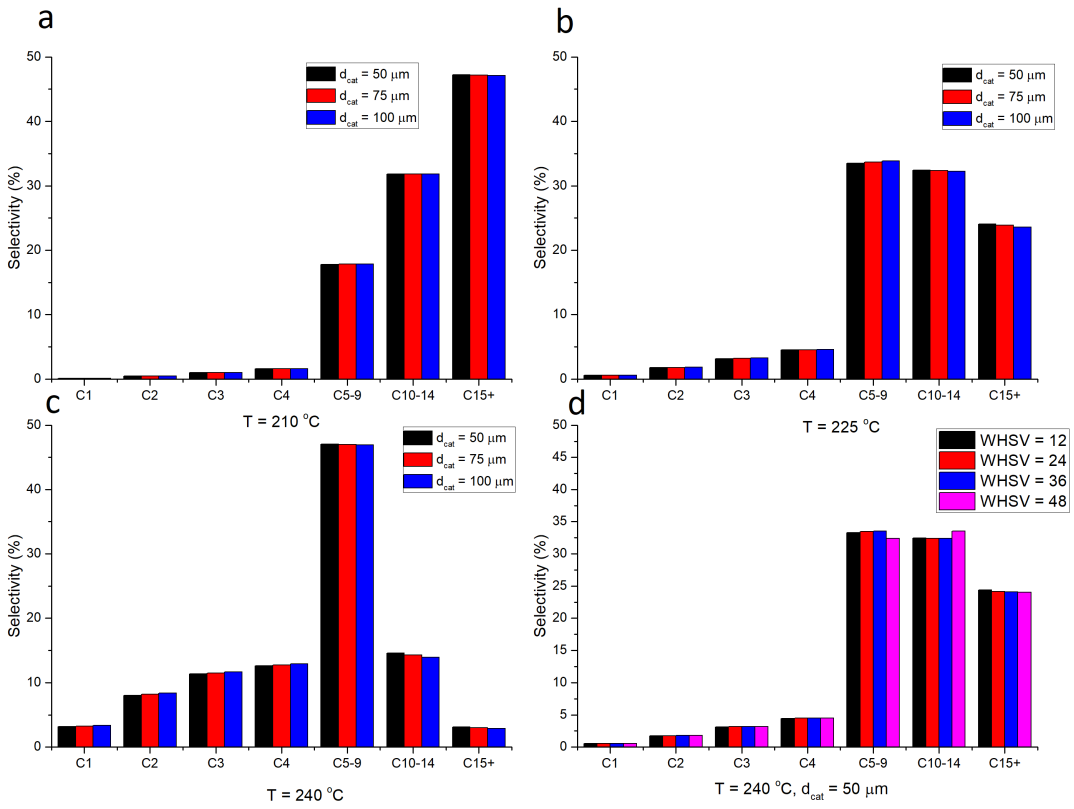

Figure 4.16: a: Effect diffusion length on FTS selectivity of powder catalysts on 210 ^oC b: 225 ^oC, c: 240 ^oC, Effect of flow rate on FTS selectivity for 50 μm powder catalysts

Figure4.16-a shows no effect of intra-particle diffusion limitations for the powder catalysts on a temperature of 210 ^oC. On higher temperatures there are some minor effects of intra-particle diffusion limitations. This shows that for powder catalysts diffusion limitations occur but are only observed on higher temperatures and are quite small. The effect of these minor diffusion limitations on the selectivity are similar to the foam catalysts.

Comparison of modeled results for foam and powder catalysts

Figure 4.17 shows the effect of flow rate and temperature on the conversion of both powder and foam catalysts. By comparing the modeled results of the activity for powders and foams it is seen that the foam catalyst have a higher performance compared to powder catalysts. The performance difference is most clearly shown on higher temperatures and lower flow rate. The lower performance of powder catalysts is due to the lower inter facial area of the powder catalyst. The foam catalyst has a set inter facial area independent of washcoat thickness, the powder catalyst is diluted to match the amount of cobalt in the foam catalyst. Figure 4.17 shows the differences in conversion for foam and powder catalysts.

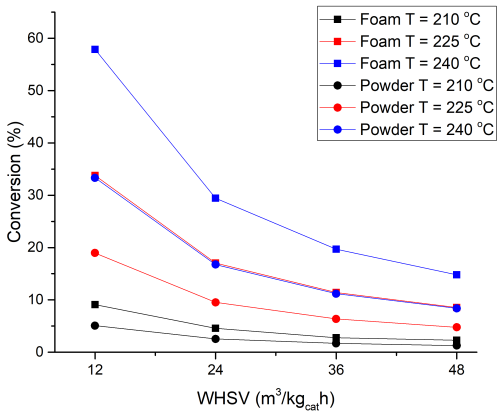

Figure 4.17: The effect of WHSV for 17 μm foam and 50 μm powder on different temperatures.

Comparing the modeled selectivities in Figures4.14 and 4.16 of foam and powder catalysts shows that on 210 ^oC there is no effect of diffusion limitations for powder catalysts while for foam catalysts there is a small effect. On higher temperatures the differences in selectivity show diffusion limitations, compared to foam catalysts the differences in selectivity for powder catalysts are smaller. The differences in selectivity between catalysts types is due to the higher conversion achieved for foam catalysts, causing larger differences in H_2/CO ratio over the length of the reactor.

Chapter 5

Conclusions

The goal of this study was to gain insight in diffusion limitations in FTS foam catalyst in comparison to powder catalyst. Activity tests of both catalysts did not give the wanted result due to a low activity for both catalysts. The powder catalysts showed some activity for FTS by the formation of measurable products and formation of wax on the catalyst. The performance of the catalysts was heavily influenced by CO_2 formation of the WGS reaction. The WGS reaction occurs parallel to the FTS which increases the conversion without the formation of desired products. Due to the low FTS productivity an effect of intra-particle diffusion limitations was not observed for the powder catalyst. The calculation of the Carberry number showed that for the catalysts external diffusion limitations were negligible. The low FTS activity of the catalyst is due to the insufficient size of cobalt active phase on the catalyst. Foam catalysts turned out to be inactive for FTS, why the foam catalysts were inactive remains unknown. The inactivity is most likely due to the small cobalt particle size on the foam catalysts, although this is not certain since the particle size of cobalt on the foam catalyst was not measured. TGA measurements on the catalysts show that the both the foam and powder catalyst produce catalyst contains a large quantity of wax. This indicates that the catalyst produces mostly long immeasurable hydrocarbon chains. Since it is impossible to collect these hydrocarbon chains, the products are considered as carbon deposition and do not contribute to the selectivity of the reaction.

Activity test were influenced by the high unbalanced achieved in the reaction. Why these unbalanced occurred remains unknown. Suggested that these unbalanced could be caused due to the large formation of wax products which stay on the catalyst surface or in the inert γ-alumina filling.

Modeling of FTS catalyst gave some insight in intra-particle diffusion limitations in the FTS. For both catalyst types diffusion limitations occurred on high temperatures. For foam catalysts this resulted in a decrease of conversion and changes in selectivity for powder catalysts only the selectivity was slightly affected. The differences are caused by the differences in internal volumes where the diffusion limitations occurred.

The overall performance of the foam catalysts was higher than the powder catalyst due to a

higher conversion. Comparing to powder catalysts to foam catalyst shows that intra-particle diffusion limitations occur faster in foam catalysts. Selectivity of the FTS was mostly influenced by temperature effects rather than diffusional effects due to the low activity of the produced catalysts.

Chapter 6

Recommendations

Several recommendations are made to further improve the study for intra-particle diffusion limitations in FTS. The activity tests were largely influenced by the unbalance in the reactor. This unbalance is most likely the result of wax formation in the pores of the support. The unbalances in the experimental results needs to be decreased in order to gain a better insight in performances of both powder and foam catalysts.

These unbalanced can be decreased by changing reactor conditions. By increasing the H_2/CO ratio and temperature and by decreasing the pressure in the reactor, the chain growth probability decreases leading to an increase in measurable products. Modeling of foam catalyst show a low conversion of CO under experimental conditions especially for the low temperature results. This may lead to immeasurable amount of product formation. To better assess the effect of diffusion limitations a higher amount of cobalt in the reactor is recommended. This can be achieved by increasing the amount of catalyst in the reactor or increase the loading on the reactor.

It is also recommended to increase the performance of the catalysts. An increase in activity will lead to higher temperatures inside the catalyst due to the exothermic nature of the reaction. This will then lead to a drop in WGS activity and increase in measurable wanted products which will be beneficial for the assessment of diffusion limitations in FTS. The performance could be increased by increasing the size of the cobalt active phase on the catalyst. From catalyst characterizations it can be seen that the cobalt powder catalysts are active but not optimal due to a small size of cobalt particles on the catalyst. It is recommended to improve the performance of the powder catalyst by increasing the size of the cobalt particles in the catalyst. This result can be acquired by increasing the cobalt loading of the catalyst. The increase in size of the cobalt active phase van be acquired by changing the impregnation method of cobalt for the catalyst. Decreasing the volume of the aqueous phase in the used deposition precipitation method is also another option in increasing the size of the cobalt active phase on the catalyst. Another possibility to improve the activity of the catalyst is to add promoters which increase activity for FTS or decrease the activity for the WGS reaction.

Modeling results show that there are small intra-particle diffusion limitations in the reactor system for both foam and powder catalyst. To give a better indication of diffusion limitations on

foam and powder catalyst a larger diffusion length is required and thus it is recommended that a larger range in particle size and washcoat thickness need to be used in order to assess the effect of intra-particle diffusion limitations for both catalyst types.

Improvements on the model can be made to make it more realistic towards experiments. A single correlation for mass transfer in packed beds was used. Most likely the behavior of mass transfer is different for foam and powder catalysts. Therefore it is recommended to improve the model adding mass transfer correlations for both powder and foam catalysts. Pressure drop is not modeled in the reactor, an advantage of foam catalysts over powder catalyst is less loss of pressure drop in the reactor. It is recommended to add pressure drop to the model, to give a larger distinction between the performance of foam versus powder catalysts. Both the reactor-and the particle model were modeled isothermal. This is unrealistic due to the high exothermic reaction enthalpy. The model can be made more realistic by adding temperature balances in both models. The influence on washcoat thickness on the interfacial surface area was not taken into account for to further improve the model it is recommended to add the effect of washcoat thickness on the inter facial surface area. It is recommended that the WGS reaction should be taken into account in the modeling of the FTS since the WGS has had a large effect on the acquired results.

Bibliography

[1] Enrique Iglesia. Design, synthesis, and use of cobalt-based fischer tropsch synthesis catalysts. *Applied Catalysis A: General*, 161:59–78, 1997.

[2] John Nijenhuis David Vervloet, Freek Kapteijn. Fischer tropsch reactionâĂŞdiffusion in a cobalt catalyst particle: aspects of activity and selectivity for a variable chain growth probability. *Catalysis Science and Technology*, 2:1221–1233, 2012.

[3] Andreas Jess Ferdinand Pohlmann. Interplay of reaction and pore diffusion during cobalt-catalyzed fischer tropsch synthesis with co2-rich syngas. *Catalysis Today*, 275:172–182, 2016.

[4] Hak-Joo Kim Jung-Il Yang, Jung Hoon Yang. Highly effective cobalt catalyst for wax production in fischer tropsch synthesis. *Fuel*, 89:237–243, 2010.

[5] Hong-Wei Xiang Yi-Ning Wang, Yuan-Yuan Xu. Modeling of catalyst pellets for fischer-tropsch synthesis. *Ind. Eng. Chem. Res.*, 40:4324–4335, 2001.

[6] Dong Hyun Chun Jung Hoon Yang, Hak-Joo Kim. Mass transfer limitations on fixed bed reactor for fischer tropsch synthesis. *Fuel Processing Technology*, 91:285–289, 2010.

[7] M. F. M. Post A. C. van 't Hoog J. K. Minderhoud S. T. Sie. Diffusion limitations in fischer-tropsch catalysts. *AIChE Journal*, 35:1107–1115, 1989.

[8] Anders Holmen Erling Rytter. On the support in cobalt fischer tropsch synthesis emphasis onalumina and aluminates. *Catalysis Today*, 275:11–19, 2016.

[9] Andrei Y. Khodakov. Fischer tropsch synthesis: Relations between structure of cobalt catalysts and their catalytic performance. *Catalysis Today*, 144:251–257, 2009.

[10] Vitaly V. Ordomsky Kang Cheng, Mirella Virginie. Pore size effects in high-temperature fischer tropsch synthesis over supported iron catalysts. *Journal of Catalysis*, 328:139–150, 2015.

[11] Thomas Tureka Henning Becker, Robert GÃijttel. Experimental evaluation of catalyst layers with bimodal porestructure for fischer tropsch synthesis. *Catalysis Today*, 275:155–163, 2016.

[12] Robert Guttel Henning Becker and Thomas Turek. Optimization of catalysts for fischer tropsch synthesis by introduction of transport pores. *Chemie Ingenieur Technik*, 86:544–549, 2014.

[13] Luca Liettia Laura Fratalocchia, Carlo Giorgio Viscontia. Exploiting the effects of mass transfer to boost the performances of co al2o3 eggshell catalysts for the fischerâĂŞtropsch synthesis. *Applied Catalysis A: General*, 512:36–42, 2016.

[14] Hong Xu Xiang Ying, Li Zhang. An experimental study on a microchannel reactor for fischer tropsch synthesis. *Energy Procedia*, 61:1394–1397, 2014.

[15] Kamyar Keyvanloo Basseem B. Hallac. An optimized simulation model for iron-based fischer tropsch catalyst design: Transfer limitations as functions of operating and design conditions. *Chemical Engineering Journal*, 263:268–279, 2015.

[16] Robert Guttelb Henning Becker and Thomas Turek. Enhancing internal mass transport in fischer tropsch catalyst layers utilizing transport pores. *Catalysis Science and Technology*, 6:275–288, 2016.

[17] V.K. Kaushik Ch. Sivaraj, P. Kanta Rao. Esca characterization of copper/alumina catalysts prepared by deposition precipitation using urea hydrolysis. *Applied Surface Science*, 51:27–33, 1991.

[18] Peter Munnik Petra E. de Jongh and Krijn P. de Jong. Recent developments in the synthesis of supported catalysts. *Chem. Rev.*, 115:6687–6718, 2015.

[19] Toshitaka Ota Hidero Unuma, Shinichi Kato. Homogeneous precipitation of alumina precursors via enzymatic decomposition of urea. *Chem. Rev.*, 115:6687–6718, 2015.

[20] Sigrid Erib Oyvind Borg, Edd A. Blekkan. Effect of calcination atmosphere and temperature on gamma al2o3 supported cobalt fischer tropsch catalysts. *Topics in Catalysis*, 45:1–4, 2007.

[21] Rachid Oukaci Sonia Hammache, James G. Goodwin Jr. Passivation of a co ru gamma-al2o3 fischer tropsch catalyst. *Catalysis Today*, 71:361–367, 2002.

[22] Valerie Meille. Review on methods to deposit catalysts on structured surfaces. *Applied Catalysis A: General*, 315:1–17, 2006.

[23] M.A.Leon Matheus. Catalytic foam stirrers for multiphase processes. *Technische Universiteit Eindhoven*, 2012.

[24] Roman Tschentscher. Rotating solid foam reactors mass transfer and reaction rate. *Technische Universiteit Eindhoven*, 2012.

[25] Jr D. Thoenes and H. Kramers. Mass transfer from spheres in various regular packings to a flowing fluid. *Chem. Eng. Sci.*, 8:271–283, 1958.

[26] H. Scott Fogler. *Elements of Chemical Reaction Engineering*. Pearson Educations, Inc, 2006.

[27] R. Krishna C. Maretto. Modelling of a bubble column slurry reactor for fischer tropsch synthesis. *Catalysis Today*, 52:279–289, 1999.

[28] J. P. Du Plessis J. G. Fourie. Pressure drop modelling in cellular metallic foams. *Chem. Eng. Sci.*, 57:2781–2789, 2002.

[29] Herman P. C. E. Kuipers G. Leendert Bezemer, Johannes H. Bitter. Cobalt particle size effects in the fischer tropsch reaction studied with carbon nanofiber supported catalysts. *J. Am. Chem. Soc.*, 128:3956–3964, 2006.

[30] Guido Mul Javier Perez Ramirez, Rob J Berger. The six flow reactor technology a review on fast catalyst screening and kinetic studies. *Catalysis Today*, 60:93–109, 2000.

Nomenclature

- Alphabetical:
  - $A_{0,r}$: Cross sectional area of the reactor $[m_r^2]$
  - a_{gs}: Interfacial surface area $[m_i^2/^m 3_r]$
  - a: Temperature dependency of the reaction kinetics $[mol/s/kg_cat/bar^2]$
  - b: Temperature dependency of the reaction kinetics $[[bar^{-1}]]$
  - C_i: Concentration of component i $[mol/m^3]$
  - ΔE_a: Difference in activation energy of initiation and termination $[J/mol]$ - D_{AB}: Bulk diffusion coefficient $[m^2/s]$
  - D_i: Diffusion coefficient of component i $[m^2/s]$
  - D_i^{eff}: Effective diffusivity of component i $[m^2/s]$
  - d_{pore}: Diameter of foam pore & washcoat pore diameter & catalyst pore diameter $[m]$
  - d_{strut}: Strutt thickness $[m]$
  - d_{wc}: Washcoat thickness $[m]$
  - F_i: Molar flow rate $[mol/s]$
  - h: heat transfer coefficient $[W/m^2K]$
  - k_{gs}: mass transfer coefficient $[m/s]$
  - k_α: Rate constant selectivity $57.6 * 10^{-3}[-]$
  - n: Reaction order $[-]$
  - m_{wc}: Mass of applied washcoat $[kg]$
  - m_{cat}: Mass of catalyst in the reactor $[kg_cat]$
  - P_i: Partial pressure of i $[Pa]$
  - r_{fts}: FTS reaction rate $[mol/kg_{cat}s]$
  - r_{obs}: Observed reaction rate $[mol/s]$
  - S_i: Selectivity component i $[-]$
  - S_i': Adjusted selectivity of component i $[-]$
  - T: Temperature $[K]$
  - $V_{foampiece}$: Volume of the foampiece $[m^3]$
  - X_i: Conversion of component i $[-]$
  - $WHSV$: Weight Hourless Space Velocity $[m^3/kg_cat/h]$

- Greek symbols: - α: ASF chain growth probability $[-]$
  - β: order chain growth probability $[-]$
  - $\epsilon_{cat,bed}$: Catalyst fraction in the packed bed $[m_{cat}^3/m_s^3]$
  - ϵ_f: Porosity of the alumina foam $[-]$
  - ϵ_s: Solid fraction in the reactor $[m_s^3/m_r^3]$
  - ϵ: Porositiy of the catalyst $[-]$
  - χ: Tortuosity of the foam piece $[m]$ - Φ_v: Volumetric flow rate $[m^3/h]$
  - ρ_{wc}: Washcoat density $[kg/m^3]$
  - γ: Shape factor for mass transfer $[-]$
  - λ: Thermal conductivity $[W/mK]$

- τ: Tortuosity of the catalyst $[-]$ - ν: Stochiometry of the reaction $[-]$

- Dimensionless numbers: - Ca: Carberry number
  - Re: Reynolds number
  - Nu: Nusselt number
  - Sh: Sherwood number
  - Pr: Prandtl number
  - Sc: Schmidt number

-

Abbreviations

- FTS: Fischer Tropsch Synthesis
- SBC: Slurry Bubble Column
- PFR: Packed Bed Reactor
- ASF: Anderson Schultz Flory
- C5+: hydrocarbon length of 5 and longer
- WGS: Water Gas Shift
- HC: Hydrocarbon

Appendices

Carberry number:

$$Ca = \frac{r_{obs}}{a_{gs} k_{gs} c_{bed}} < \frac{0.05}{|n|} \tag{1}$$

where a_{gs} is:

$$a_{gs} = \frac{6\epsilon_s}{d_{cat}} \epsilon_{cat} \tag{2}$$

$$r_{obs}(T = 225^o C, d_{cat} = 75\mu m) = (F^{mol}_{CO,in} - F^{mol}_{CO,out}) * 10 = 2.35 * 10^{-5} [kmol/kg_{cat} s] \tag{3}$$

$$Ca = \frac{2.35 * 10^{-5}}{\frac{6}{75e-6} * 0.64 * 0.0182 * 0.0104 * \frac{200-199.9}{200}} = 0.0055 \tag{4}$$

- Results BET:

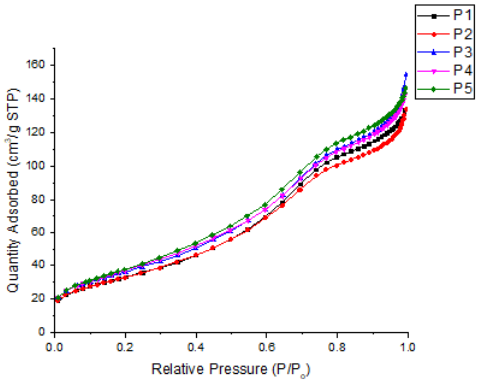

- Results TEM:

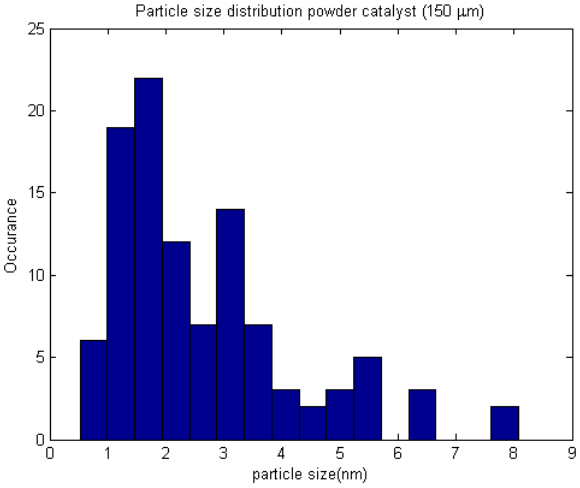
Particle size distribution powder catalyst (150 µm)
Occurance
particle size(nm)
0
5
10
15
20
25
0
1
2
3
4
5
6
7
8
9

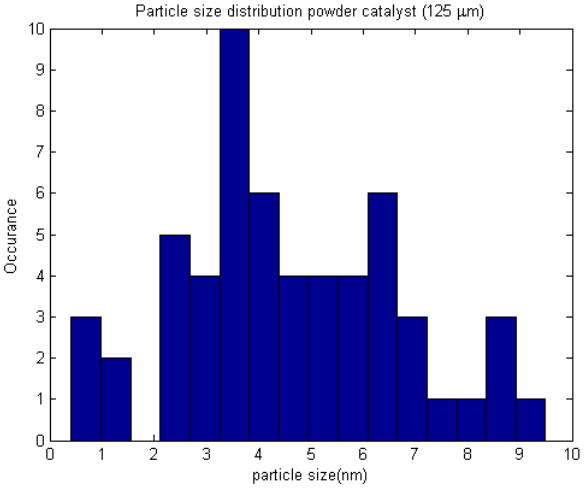
Particle size distribution powder catalyst (125 µm)
Occurance
particle size(nm)
0
1
2
3
4
5
6
7
8
9
10
0
1
2
3
4
5
6
7
8
9
10

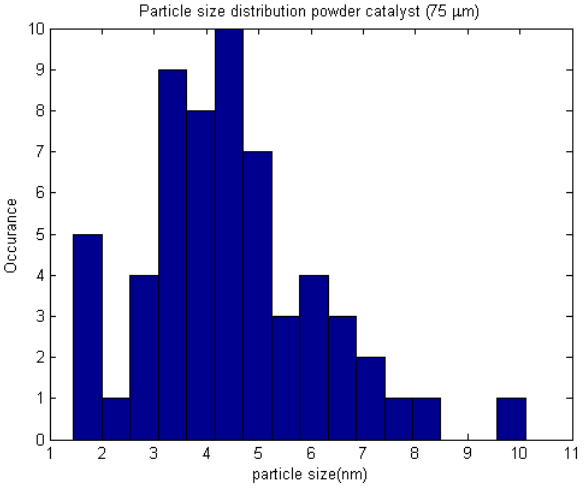
Particle size distribution powder catalyst (75 µm)
Occurance
particle size(nm)
0
1
2
3
4
5
6
7
8
9
10
1
2
3
4
5
6
7
8
9
10
11

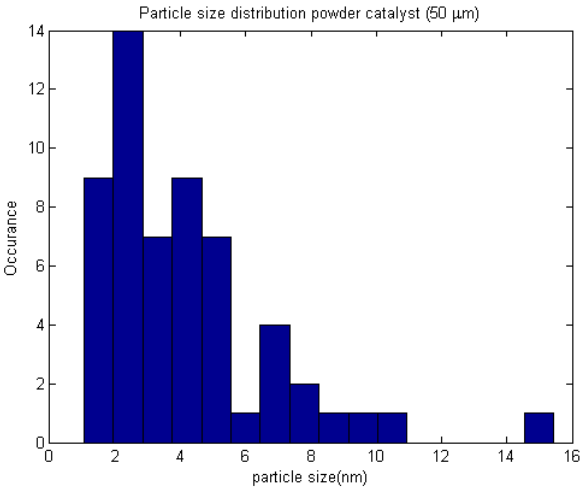
Particle size distribution powder catalyst (50 µm)
Occurance
particle size(nm)
0
2
4
6
8
10
12
14
16